On the optimization of LUMIO-LPF tracking windows using LiAISON

Literature Study

Master Thesis

Thomas Bosboom

Delft University of Technology

TU Delft

This page is left blank intentionally.

On the optimization of LUMIO-LPF tracking windows using LiAISON

Literature Study

by

Thomas Bosboom

In partial fulfillment of the requirements for the degree of

Master of Science
in Aerospace Engineering
at Delft University of Technology

Student number: 4787196
Project duration: September 2023 until March 2024
Supervisor Dr. ir. S. Speretta TU Delft, Daily Supervisor

TU Delft

Contents

List of Symbols

Symbol	Definition	Unit
$A(t)$	Linear dynamics matrix	[-]
$\boldsymbol{B}$	Bias covariance matrix	[-]
$\boldsymbol{B}$	A priori the measurement biases estimate	[-]
$\boldsymbol{C}$	Cross-covariance matrix	[-]
C_j	Jacobi constant	[-]
$\boldsymbol{f}$	(Non)-linear dynamics function	[-]
$\boldsymbol{h}$	(Non)-linear measurement function	[-]
$\tilde{\boldsymbol{H}}$	Jacobian of the measurement	[-]
i	i-th measurement in a measurement session	[-]
$\boldsymbol{K}$	Kalman gain matrix	[-]
k	k-th measurement session or fit span	[-]
$\boldsymbol{N}$	Information state vector	[-]
$\boldsymbol{N}$	Measurement bias vector sensitivity matrix	[-]
$\boldsymbol{P}$	Error covariance matrix	[-]
$\boldsymbol{Q}$	Process noise covariance matrix	[-]
$\boldsymbol{R}$	Measurement noise covariance matrix	[-]
S	Measurement sensitivity	[-]
$\boldsymbol{T}$	Body-to-inertial frame rotation matrix	[-]
$\boldsymbol{v}$	Random process noise	[-]
$\boldsymbol{W}$	Measurement noise covariance matrix	[-]
$\boldsymbol{w}$	Random measurement noise	[-]
$\boldsymbol{x}$	State vector	[-]
$\Delta\boldsymbol{x}$	State deviation vector	[-]
$\Delta\boldsymbol{y}$	Measurement deviation vector	[-]
λ	Eigenvalue	[-]
$\boldsymbol{\Lambda}$	Information matrix	[-]
$\boldsymbol{\Phi}$	State transition matrix	[-]
ϕ	Relative azimuth angle between two spacecraft	[rad]
ψ	Relative elevation angle between two spacecraft	[rad]
σ	Standard deviation	[-]

List of Figures

List of Tables

Introduction

Smallsats have become increasingly popular for a variety of space applications due to their low cost, compact size, and versatility. Recent literature suggests that there is a large relevance for cislunar smallsat missions such as the Lunar Meteoroid Impact Observer (LUMIO) [1], Cislunar Autonomous Positioning System Technology Operations and Navigation Experiment (CAPSTONE) [2] and EQUilibriUm Lunar-Earth point 6U Spacecraft (EQUULEUS) [3]. However, the growing amount of satellites poses a challenge to existing ground networks, such as the Deep Space Network (DSN) [4, 5]. This requires new innovations that enable the need to direct-to-Earth communications. Omitting the use of ground stations can lead to potential benefits related to the reduced communication power requirements and reduced operational costs [5, 6, 7, 8]. Furthermore, though it is a small effect for cislunar missions, the inherent delay of ground station transmissions for deep space missions precludes understanding of the real-time state [9]. Lastly, future lunar missions could be located at sites on the Moon where direct communication links to Earth are not possible that will require a relay satellite to gain access to Earth [5, 10, 11].

One way to accommodate these challenges is by exploring autonomous orbit determination (AOD) techniques. This enables smallsats achieve precise positioning without the direct need for a ground station or other type of beacon [5, 12]. One such technique is called Linked Autonomous Interplanetary Satellite Orbit Navigation (LiAISON) [13]. It is one of the effective techniques for smallsats because it is straightforward and uses existing radio communication technologies [14, 12]. To enable smallsats to autonomously navigate through space, LiAISON utilizes at least one satellite-to-satellite (SST) measurement type to obtain the simultaneous absolute states of at least two satellites where at least one of the satellite orbits has a unique size, shape, and orientation due to an asymmetric gravity field [15]. As direct-to-Earth navigation gets more difficult when a satellite gets further away from Earth, AOD could also be useful for satellites further than the Earth-Moon system [16]. The thesis will consider the mission scenarios of the LUMIO mission because of its large knowledge framework within TU Delft. Precise navigation is critical for a multitude of applications, such as remote sensing, station-keeping (S/K), and even for allowing human space travel [16]. While LiAISON can provide accurate state estimates, the complexity of the orbit dynamics and estimation filtering could have a substantial role in the timing of measurements between the satellites [15, 17, 6]. Also, state uncertainty builds up differently under different dynamics [18]. Navigation accuracy can additionally effect the accuracy and timing of S/K maneuvers and vice versa [19, 5]. These parameters could lead to an optimal set of time windows throughout which the spacecraft performs orbital determination measurements while maintaining a certain accuracy. This timing was conducted on a simplified circular restricted three body problem (CRTBP) and over a period of just three weeks [20]. To maximize the navigation filter's performance, timing is critical for gathering the most insightful observations [20]. The goal of this proposed thesis work is to find an optimal tracking timing strategy using higher fidelity dynamic models and propagate an AOD scenario over the mission duration of LUMIO of 1 year.

The layout of this literature study starts by addressing the current trends and challenges in Chapter 1. From this follow the fundamentals related to orbit determination in Chapter 2. Then, the potential scientific contribution that the this project can contribute to are described in Chapter 3. Finally, the conclusions are elaborated upon in Chapter 4.

1

Trends in cislunar missions

A new era of small satellites for space exploration comes with a growing demand for autonomous orbit navigation (AOD). This reduces dependency on ground-based tracking and provides a significant reduction in operational costs due to overcrowded communication networks [12]. First, a general overview of existing cislunar smallsat missions is given in Section 1.1. Cislunar missions operate with different orbits types that posses different properties. This is elaborated upon in Section 1.2. The LUMIO mission is touched upon in Section 1.3, followed by an explanation of the workings of LiAISON in Section 1.4.

1.1. Current cislunar missions

The availability of low-cost and low-volume commercially-of-the-shelf (COTS) spacecraft subsystems have enabled the miniaturization in the space sector and commercial viability for missions using small-scale products with applications that we considered impossible before [21]. With the current developments in the field of spacecraft miniaturization, more players have entered the satellite industry [22]. Turan et al. [12] looked at a total of 64 missions and concluded that, as of April 2022, most deep-space missions are focused on the Moon. The majority of the 64 missions aim to characterize the surface or atmosphere of a body. 34 out of the 64 missions incorporate inter-satellite links for telemetry, telecommand, or navigation purposes. Of these 34, the majority of 22 operates in cislunar space. For the sake of a proper delineation of the topic of the thesis work, it might be useful to only consider cislunar missions. Below one can find an overview of smallsat cislunar missions [12].

	Inter-Satellite Link (ISL)	**Direct-to-Earth Link (DTE)**	**Inter-Satellite Link (ISL) + Direct-to-Earth Link (DTE)**
Cislunar Missions	LUMIO, VMMO, CLE*, MoonCare*, NanoSWARM	Lunar Flight Light, Lunar Ice Cube, LunaH-Map, LunIR, ArgoMoon, OMOTENASHI, Cislunar Explorers*, EQUULUES, HALO, WATER, IMPEL, CubeX	MiLuV, BOLAS*, OLFAR**, DSL**, CAPSTONE
Total	5	12	5

Table 1.1: Overview of communication link configurations for different cislunar smallsat missions. (*) = constellation of two satellites and (**) = constellation of more than two satellites. Source: [12].

The majority of the issues related to the use of satellite navigation are:

- **Limited power**: Only a limited amount of power is budgeted to communication in general [12]. This naturally leads to limited power availability for navigation. Atmospheric effects can play a role in the effectiveness of radiometric Earth-satellite communication, where the specific cause of interference and the received bit energy-to-noise ratio or BER depend on parameters such as signal frequency and transmitted power from the satellite [23, 24]. Additionally, SST tracking happens over smaller distances than contact with Earth, yielding an overall smaller free-space path loss [5].
- **Limited contact time**: More spacecraft could be tracked at only a limited contact time. This is related to the ground station ”visibility problem” which is about the communication conflicts that occur when

multiple satellites try to communicate with ground stations in the visible range. As the amount of satellites increases, the more challenging the visibility problem becomes. The degree depends on the altitude and antenna parameters [25]. The communication time could affect the degree to which a spacecraft is at its intended location and thus the accuracy of station-keeping (S/K) maneuvers [26].

- **Ground station delays**: Commands from ground stations are prone to atmospheric delays of the signal propagation. There is a certain downtime between signal from satellite causing a deviation from the true and target states [23].
- **Mission event schedule**: Body to communicate with might not be available due to their own internal communication scheduling [26].

Spacecraft autonomy can lead to decreased costs if ground control operations or hardware are reduced or eliminated [15, 7]. Since most navigation is based on a radiometric Earth-satellite link, there is a possibility to use this existing technology to automate the navigation aspect by performing satellite-to-satellite tracking (SST) [12]. This could also be beneficial because the relatively lower power signal of smallsat is not obscured by Earth's atmosphere and there is no direct-to-Earth (DTE) contact for all satellites that are not the relay. Another benefit might be that increased navigation might lead to a decreased quantity of ΔV required for S/K maneuvers.

1.2. Cislunar orbit types

The Earth-Moon system offers a variety of orbits for cross-link radiometric navigation. Next to Lunar and Earth orbits such as LEO, GEO, polar and Elliptical Lunar Frozen Orbit (ELFO), there are also halo orbits [27, 28]. Halo orbits or Libration Point Orbits (LPOS) are located around the collinear libration points (L1, L2 and L3) [28]. One of the advantages of L2 halo orbits is that some of these can provide great coverage of the lunar far-side and polar regions without blocking the visibility to Earth [29]. Additionally, orbits around the L2 libration points are appropriate for LiAISON because they are locally unique and consistently stay in locations with a high degree of asymmetry in the third-body perturbation of the Moon [15].

When a halo orbit is derived from the CRTBP, the orbit can be called periodic for a reasonable length of time. However, high-fidelity models (n-body dynamical systems) allow such an orbit to deviate from the periodic case in a relatively short time frame motion due to perturbations of external bodies. For that reason, it is called "quasi-periodic" [15, 26]. The geometry of a halo orbit depends on the Jacobi energy of the spacecraft, C_j [28]. The smaller C_j, the larger the orbit [30].
Equation 1.1 is related to Equation 2.1 and represents the total energy of the tertiary mass (the spacecraft) relative to the non-dimensional rotating reference frame.

$$C_j = 2\left(\frac{1-\mu}{r_1} + \frac{\mu}{r_2}\right) + x^2 + y^2 - \left(\dot{x}^2 + \dot{y}^2 + \dot{z}^2\right) \tag{1.1}$$

Near Rectilinear Halo Orbits (NRHOs) are a subset of the halo families that make close approaches to the smaller body (the Moon) [26]. For example, the CAPSTONE mission makes use of such an orbit [3]. The stability index is smaller for a NRHO compared to that of the nominal halos [30]. There are also orbits that move around the L_1 and L_2 Lagrangian points but lie entirely in the xy-plane of the Earth-Moon CRTBP, the distant retrograde and Lyapunov orbits [31]. Turan et al. [6] performed analysis specific to the LUMIO (L2 halo)-LPF (ELFO) constellation and showed that the best position observability occurs at moments when LPF is in the high-velocity region, so periselene of its ELFO. K. A. Hill [15] simulated a large variety of constellation geometries and concluded that Halo-Moon constellations provide the best observability effectiveness under the conditions shown below. More on measurement observability in Chapter 2.

- Spacecraft should have relatively large separation distances.
- Not all the spacecraft can remain in the same plane for their entire trajectories.
- Libration orbits with shorter periods lead to quicker convergence. This was found by Turan et al. too [32].

1.3. LUMIO cubesat mission

LUMIO is a 12U cubesat this aims to detect micro-meteorite impacts on the far side of the moon to full the knowledge gab on the thus far unobserved impact events in the 10^{-4} to 10^{-1} kT TNT equivalent kinetic energy

range while also testing the hypothesis of asteroid impact asymmetry between the lunar nearside and far side [1].

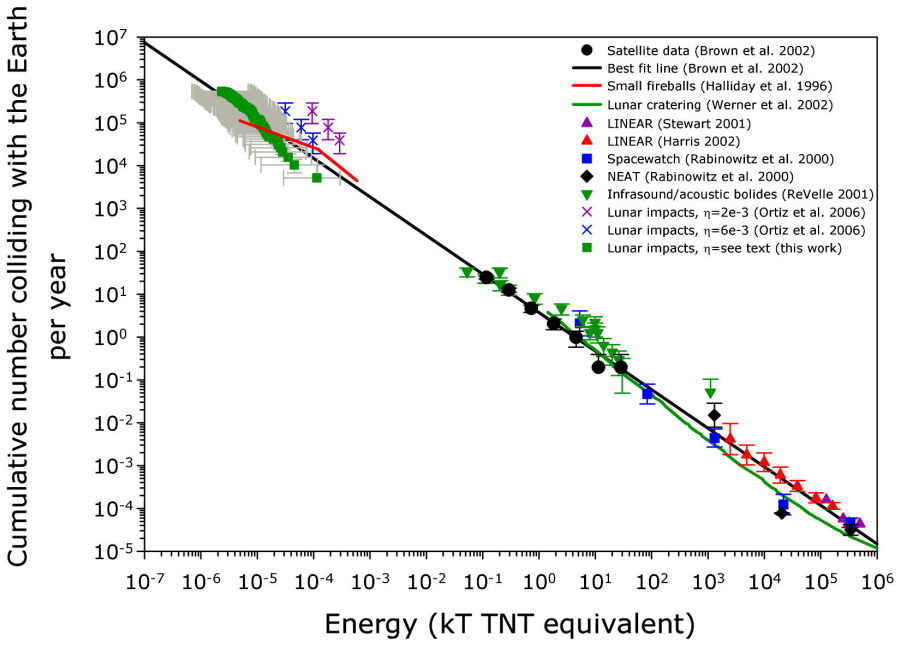

Figure 1.1: Scientific knowledge gab of meteorite impact events in the 10^{-4} to 10^{-1} kT TNT equivalent kinetic energy range. Source: [33]

Its payload, the LUMIO-cam allows for the detection of flashes on the lunar surface. A consistent image of the lunar far side is made sure by means of orbiting in a southern quasi-periodic orbit around the Earth-Moon L2 Lagrange point. The advantage compared to ground observations is that the observations are not prone to atmospheric effects and the spacecraft can provide a complete view of the lunar full-disk at once [30]. The main means of communications is through DTE links, but radiometric inter-satellite is established between LUMIO and the SSTL Lunar Pathfinder (LPF) [30]. The LPF is a spacecraft with the purpose to enable connection with future Lunar assets. Payload data is not transmitted through the LUMIO-LPF link, but through the primary Earth connection. The (inter-satellite link) ISL between the two satellites serves as a redundant commanding link [6]. During the operational lifetime of 1 year, LUMIO's operations are split into two phases: The phase is divided in two phases: the science cycle, and the navigation and engineering cycle. It involves the orbit determination and subsequent station-keeping maneuvers required to maintain the right conditions during the science cycle [1].

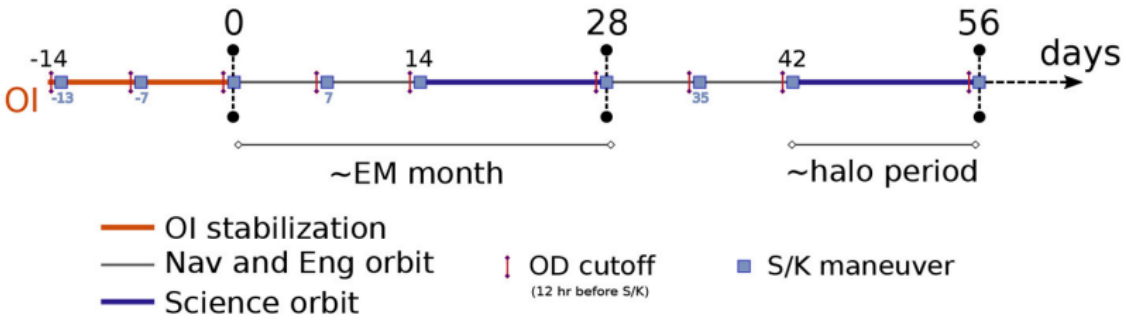

Figure 1.2: Timing strategy employed for station-keeping maneuvers. Source: [30]

The navigation and engineering cycle is of the largest relevance for this thesis. Previous master theses have already performed work on the topic [34, 35, 36, 37, 38, 39]. Note that Figure 1.2 shows that there are S/K maneuvers that have to be performed. The amount accuracy of these maneuvers depends on the accuracy of the OD, so it is of best interest to reduce uncertainty as much as possible to keep the ΔV low [40].

LUMIO will show the AOD capabilities of smallsats and show the ability to provide useful scientific data from interplanetary missions using COTS smallsat technologies [1]. It will be a technology demonstrator for the LiAISON.

1.4. LiAISON-based navigation

There exists a variety of navigation methods, those that store data on-board and those that send data to a ground station to be analyzed and get feedback [12]. There are two types of navigation [41]:

- **Absolute**: Information on the orbit states is known with respect to an inertial reference.
- **Relative**: Information on the orbit states is defined with respect to a moving reference point such as another satellite. To obtain the absolute information one needs knowledge of the absolute position of the moving reference point.

Relative measurements, in a two-body problem, do not provide the absolute orientation of the orbital planes but only the relative orientation because the orbits cannot be fully unique [8]. That is, the absolute states of one spacecraft cannot be known as a particular initial condition can lead to multiple trajectory outcomes. At least one beacon must be added to produce a reference to the inertial frame as a result from the rank deficiency problem [41, 42]. Examples of this are introducing GPS [43, 44], measuring with respect to known stars [45], lunar landmarks [46, 47] or incorporating a third satellite with an orbit that is optimized for observability [9]. These examples are based on a two-body system, i.e. Earth-satellite or Moon-satellite.

However, it is possible to obtain absolute state information, so solving the rank deficiency problem, without the need for a second type of sensor. Under certain circumstances, LiAISON provides that solution by simultaneously obtaining the absolute states of at least two bodies [15]. Hence the name ”liaison”, which stands for ”mutual understanding”. The effectiveness level of LiAISON depends on the level of asymmetry of the gravity field in the spacecraft’s environment. A region in three body systems where the force due to a perturbing third body is relatively large would be a good candidate for LiAISON as this leads to uniqueness in the respective orbit [15, 27]. In that case, at least one of the satellite orbits has a unique size, shape, and orientation [15, 6]. That means that the unique time history of SST observations and thus absolute states are known when the initial conditions are given [5]. The impact of the asymmetric acceleration field on the spacecraft’s trajectory must outweigh the noise from observations and the impacts of unmodeled accelerations by a large margin [15]. For that reason, libration points are a good choice, especially the unstable collinear Langrange points (L1, L2 and L3) [48, 5].

Additional advantages of cross-link radiometric navigation are that the accuracy is large and that it can be used by existing systems [49, 50]. Conventional navigation relies on the scheduling made based on the availability of the ground station [15, 50]. Omitting the ground station element could allow the spacecrafts to choose tracking time in a less constrained manner, caused by the limitations due to the ground station visibility [51]. LiAISON based navigation can be done for spacecraft that are in-orbit, but also lunar surface assets (LSA) [5]. Research has been done on a two-satellite system (Lagrange point-moon), but it can be extended to navigation systems of more than two satellites [14, 10, 11, 19, 52]. Other work was done on Lagrange point-geosynchronous constellations [53] or inter-planetary spacecraft [54, 50]. Additionally, supplementing LiAISON measurements with ground-based measurements can improve tracking performance [5, 54, 50]. The application of LiAISON in crewed missions, in which models contain a certain Unfortunate Lack of Acceleration Knowledge (FLAK), have also previously been investigated [55].

2

Fundamentals of orbit determination

Orbit determination (OD) provides an estimation of the spacecraft state vector by iteratively correcting a dynamical model to minimize residuals between measured and model states. The OD can be split into three elements: the dynamical model, measurement model, and estimation model. This chapter will cover all three of them. One should note the following content is not strictly applied to the concept of LiAISON-based navigation only. The measurement and estimation model concerns inter-satellite observables rather than the Earth-to-satellite counterparts. The intricacies of the dynamical models are explained in Section 2.1. To correct for perturbations, the dynamical model might have to be adjusted by means of station-keeping (S/K) maneuvers. Likewise, the models should consider certain occultation and solar radiation scenarios. These are both also explained in this chapter as well. The measurement and estimation models are respectively shown in Section 2.2 and Section 2.3. With the goal of improving AOD, it is important to define a metric to compare the effectiveness of measurements in the estimation process. This will be touched upon in Section 2.4. The mechanisms behind the propagation of state uncertainty are touched upon in Section 2.5.

2.1. Dynamical model

The dynamical model in the context of OD entails in a concrete sense the state propagation of a satellite in a predefined dynamical environment, depicted by a variety of forces that are exerted on the spacecraft by celestial bodies. The degree of the fidelity of the dynamical model depends on the number and type of forces that one takes into consideration. The true state is never exactly known, but the more intricate the environment, the better it represents the ”true” dynamics [56].

2.1.1. The circular-restricted three-body problem

The easiest, and most commonly employed, model is the circular-restricted three-body problem (CRTBP) [15, 19, 16, 27, 6, 28, 57]. The CRTBP is defined by the following equations of motion:

$$\begin{aligned}
\ddot{x} &= x + 2\dot{y} - \frac{(1-\mu)(x+\mu)}{r_1^3} - \frac{\mu(x+\mu-1)}{r_2^3} \\
\ddot{y} &= y - 2\dot{x} - \frac{(1-\mu)y}{r_1^3} - \frac{\mu y}{r_2^3} \\
\ddot{z} &= -\frac{(1-\mu)z}{r_1^3} - \frac{\mu z}{r_2^3}
\end{aligned} \tag{2.1}$$

$$\begin{aligned}
r_2 &= \sqrt{(x+\mu-1)^2 + y^2 + z^2} \\
r_1 &= \sqrt{(x+\mu)^2 + y^2 + z^2} \\
\mu &= \frac{m_2}{m_1 + m_2}
\end{aligned} \tag{2.2}$$

Here, x, y, and z represent the spacecraft states with respect to the Earth-Moon barycenter in a rotating reference system or synodic frame. The system contains three bodies, assigned the following properties: Earth (P_1 and $m_1 = m_E$), Moon (P_2 and $m_2 = m_M$), and the spacecraft (P_3, $m_3 = 0$). Equation 2.1 makes use to dimensionless parameters: μ represents the dimensionless mass distribution, r_1 is the distance between the P_3 and P_1, and r_2 is the distance between the P_3 and P_2. This model assumes no perturbations from

bodies other than the primary and secondary bodies, zero spacecraft mass and a time-invariant Earth-Moon distance. The model starts to diverge severely from the true dynamics due to the ignored perturbations.

2.1.2. High-fidelity model

In reality, the dynamical system is more complex because it includes a large variety of perturbing forces on the spacecraft. Because planets and moons aren't orbiting in circular, co-planar orbits in the real Solar System have no longer any periodic solutions. The same primary locations do not reoccur in any acceptable amount of time [58]. The best representation would be a "full-ephemeris" model that includes all time-dependent positions of all celestial bodies.

$$\begin{aligned} \dot{\boldsymbol{x}} &= \boldsymbol{f}(\boldsymbol{x}, t) + \boldsymbol{v} \\ \boldsymbol{y} &= \boldsymbol{h}(\boldsymbol{x}, t) + \boldsymbol{w} \end{aligned} \tag{2.3}$$

The dynamics and measurement outputs of a spacecraft is represented by a set of non-linear ordinary first order differential equations as shown in Equation 2.3.

System linearization

A number of powerful methods from the domain of linear estimation theory may be employed by converting the highly non-linear system into a linearized form [23]. Linearization refers to using the first term of the Taylor series of an otherwise non-linear function. This approximation of the dynamics can be extended to higher orders to capture some of the effects caused by non-linearities [59]. Instead of estimating the truth trajectory, $\boldsymbol{x}$, the deviations with respect to the nominal trajectory, $\boldsymbol{x}^*$, are used, depicted by state deviation vector $\delta\boldsymbol{x}$ [15]. While linearization provides an easy and fast solution, the solution does not adequately define trajectory statistics when the linearized states are propagated over a longer period of time [59].

$$\begin{aligned} \delta\boldsymbol{x} &= \boldsymbol{x} - \boldsymbol{x}^* \\ \delta\boldsymbol{x}(t) &= \boldsymbol{\Phi}\left(t, t_0\right) \delta\boldsymbol{x}(t_0) \end{aligned} \tag{2.4}$$

An asterisk indicates that the values of $\boldsymbol{x}$ and $\boldsymbol{y}$ are derived from the nominal solution from Equation 2.3 with the initial conditions $\boldsymbol{x}^*(t_0) = \boldsymbol{x}(t_0)$. Equation 2.4 is the result of linearizing Equation 2.3. The propagation of $\delta\boldsymbol{x}$ is done by using $\boldsymbol{\Phi}\left(t, t_0\right)$, the state transition matrix (STM), also known as the first order state transition tensor (STT). $\delta\boldsymbol{x}(t_0)$ is mapped onto epoch t, resulting in $\delta\boldsymbol{x}(t)$. $\boldsymbol{\Phi}\left(t, t_k\right)$ itself is the result of an ODE as shown in Equation 2.5 [23]. This is done numerically and is embedded in the software Tudatpy as will be elaborated upon in Section 2.1.5.

$$\dot{\boldsymbol{\Phi}}\left(t, t_0\right) = A(t)\boldsymbol{\Phi}\left(t, t_0\right) = \left.\frac{\partial \boldsymbol{f}}{\partial \boldsymbol{x}}\right|_{\boldsymbol{x}=\boldsymbol{x}^*} \boldsymbol{\Phi}\left(t, t_0\right) \tag{2.5}$$

Viability settings

The high fidelity model is able to model physical phenomena that are not modeled in the CRTBP. One such aspects is the effect of occultations [60, 61]. For example, the Moon can block the view of the transmitter and observer at some epochs. Likewise, the magnitude of solar radiation pressure induced acceleration (SRP) (and thus the orbital trajectory) depends on the moments in which the satellites are in a shadow caused by the Moon and Earth. Literature shows that for EM L2 orbits, Earth and Moon induced shadows occur biannually and monthly respectively [60]. Increasing the halo orbit amplitude decreases the total shadow times [60]. Although not the main concern of this work, the LUMIO could provide continuous visibility with Earth for data relay of the amplitude of its halo orbit is large enough [58].

2.1.3. Continuation models

Libration point orbits are inherently unstable when the assumptions of a CRTBP model are not incorporated. It is then not possible anymore to create a perfect continuous periodic solution of a trajectory. Numerical simulations in higher-fidelity dynamical models yield a state history in which the Lagrange point orbiter departs from the ideal periodic solution after 1 to 2 revolutions [62]. For LUMIO this equates to approximately 14 to 28 days [6].

Instead, quasi-periodic solutions can be found, commonly referred to as the quasi-periodic halo orbits, which can be used as a multi-revolution reference solution that the spacecraft should follow. These orbits

are generated by means of the ”multiple differential shooting technique” [62]. This method aims to generate adjustments to the velocity element of the state vector at the start of each patch point provided constraints, within tolerance, on position and velocity continuous between the patch points [58].

Whether such as model is required depends on the station-keeping strategy used. If these are performed within short time intervals, the true path will not deviate much from the reference solution. Over larger time intervals, the deviations are larger and requires more fuel [63]. It is a subjective question of at what deviation value the dynamical model and the continuation model states are considered close enough.

2.1.4. Station-keeping

S/K maneuvers should be incorporated in the dynamical model for a navigation framework to function successfully [5, 55, 64]. For the most realistic notion of the navigation performance, these maneuvers should then be implemented into the dynamical model [5]. It is expected that errors in the execution of S/K maneuvers will lead to a worse accuracy [5, 65]. This might demand greater adjustments required downstream. Moreover, maneuver cost are significantly influenced by the accuracy of the nominal orbits [63]. The resulting decrease in ΔV for a higher fidelity dynamic model then does come at the cost of a higher computational load [40]. The degree of corrections needed also depends on the orbit geometry. Co-linear halo orbits are inherently unstable and require more ΔV then DRO's [48, 27]. However, compared to most other cislunar orbits, L1/L2 halo orbits require low S/K propellant [61]. The amount of required ΔV for these halo orbits depends on the Jacobi energy of the orbit [30]. As the orbit becomes more energetic the annual S/K ΔV seems to decrease [66, 30]. Also, a large stability index is usually associated with large S/K costs [30]. In the context of LUMIO, a Jacobi constant of 3.09 was chosen such that the ΔV for orbit transfer plus 1 year S/K is kept minimal [30].

Algorithms will have to be incorporated to define the direction, magnitude, and timing of an impulsive ΔV maneuver. The LUMIO and EQUULEUS missions incorporate the target point method (TPM) [30, 2]. Two other methods are the differential corrector and Cauchy-Green Tensor methods [67]. The TPM method performs corrections at specified moments in time where the correction magnitude and direction is based on the deviation from the reference orbit at downstream target points [40, 68]. Figure 1.2 gives an illustration of the planned maneuver timing that employs TPM. Although the two mentioned missions the TPM method based on the first order STT (the STM), there exist a higher-order TPM method with improved sensitivity of navigation errors [69]. The specific maneuver epochs result in an excellent orbit during the science phase, but it however comes at the cost of additional required ΔV [30]. The S/K frequency versus accuracy trade-off calls for a variety of possible S/K timing strategies. It was shown that the total ΔV increases with increased time interval between corrections and increased uncertainty in the maneuver accuracy [70]. The worst-case 1-year operational S/K ΔV of the LUMIO orbit is 4.3 [m/s] (3σ) [1]. Eventually, improving the OD error could help lowering the stochastic ΔV component and save spacecraft mass.

2.1.5. Modelling software

Solar system ephemerides are not required in the CRTBP, but high-fidelity models do require information on the relative dynamics of all bodies and thus state histories. The JPL DE405 planetary ephemerides database is a good source [71]. The use of these ephemerides is common practice in literature when it concerns those higher-fidelity models [15, 27, 5]. Producing and verifying results is a qualitatively intensive process. To fulfill the objectives of this research, the results will come from Python. The TU Delft Astrodynamics Toolbox (Tudat) is used for this thesis. Tudat is a robust collection of validated astrodynamics functionalities [72]. It has been used before in previous thesis works on LUMIO [34]. Tudat's functionality is built in C++, but includes a Python wrapper, Tudatpy. Tudat integrates the NASA/NAIF Spice toolkit, which includes the JPL DE405 ephemerides. A downside of Tudat is that it is still in production and documentation is a work in progress. Another relevant TU Delft-built work is the CRTBP Autonomous Orbit Determination application, built in Matlab by Erdem Turan. While this application is built based on the CRTBP only, it can be used to validate the Tudatpy CRTBP equivalent. This equivalent is made by creating an Earth-Moon system with a perfectly circular Moon orbit and with a simple point mass acceleration model.

2.2. Measurement model

The same method of linearization as done in Section 2.1 is used for the measurement side of Equation 2.3. The measurement residuals are defined as the difference between the true observations and the observations

derived from the observation-state relationship defined in Equation 2.7 at the nominal trajectory.

$$\delta \boldsymbol{y} = \boldsymbol{y} - \boldsymbol{y}^* \tag{2.6}$$

$$\delta \boldsymbol{y}(t_i) = \tilde{\boldsymbol{H}}_i \delta \boldsymbol{x}(t_i) = \left. \frac{\partial \boldsymbol{h}}{\partial \boldsymbol{x}} \right|_{\boldsymbol{x}=\boldsymbol{x}_i^*} \delta \boldsymbol{x}(t_i) \tag{2.7}$$

Regarding timestamps, measurements are divided into fit spans defined by $k = 1, \dots m$. For every k there are measurements $i = 1, \dots \ell$. The dimension of $\tilde{\boldsymbol{H}}_i$ is dependent on the amount of measurement types that are included in the simulation and quantity of elements of the state vector. The most common observation types are range and range-rate [23]. Line-of-sight (LOS) angles are also used [14]. The inter-satellite RF measuring method is one-dimensional. To enable inter-satellite relative navigation, RF angle data are often paired with RF range measurements [49]. For the LUMIO mission it was shown that range-only measurements provide better accuracy than range-rate measurements only [6]. The three mentioned measurement types are calculated using Equation 2.8. These values are then differentiated and converted into Equation 2.9. This could be done analytically or numerically. Erdem et al. provide analytical solutions to the entries of Equation 2.9 [6].

$$\begin{aligned}
\rho &= \sqrt{(x_1 - x_2)^2 + (y_1 - y_2)^2 + (z_1 - z_2)^2} && + \rho_{bias} + \rho_{noise} \\
\dot{\rho} &= \frac{(x_1 - x_2)(\dot{x}_1 - \dot{x}_2) + (y_1 - y_2)(\dot{y}_1 - \dot{y}_2) + (z_1 - z_2)(\dot{z}_1 - \dot{z}_2)}{\sqrt{(x_1 - x_2)^2 + (y_1 - y_2)^2 + (z_1 - z_2)^2}} && + \dot{\rho}_{bias} + \dot{\rho}_{noise} \\
\phi &= \arctan\left(\frac{y_2 - y_1}{x_2 - x_1}\right) && + \phi_{bias} + \phi_{noise} \\
\varphi &= \arcsin\left(\frac{z_2 - z_1}{\sqrt{(x_1 - x_2)^2 + (y_1 - y_2)^2 + (z_1 - z_2)^2}}\right) && + \varphi_{bias} + \varphi_{noise}
\end{aligned} \tag{2.8}$$

If all measurements types are included, $\tilde{\boldsymbol{H}}_i$ would look like Equation 2.9. For range-only it is just the first row. For the purposes of this work, $\tilde{\boldsymbol{H}}_i$ more relevant. $\tilde{\boldsymbol{H}}_i$ is converted into $\boldsymbol{H}_i$ through Equation 2.10. The relevance is made clear in Section 2.3 and Section 2.4.

$$\tilde{\boldsymbol{H}}_i = \begin{bmatrix} \frac{\partial \rho}{\partial x_1} & \cdots & \frac{\partial \rho}{\partial \dot{z}_2} \\ \vdots & \ddots & \vdots \\ \frac{\partial \varphi}{\partial x_1} & \cdots & \frac{\partial \varphi}{\partial \dot{z}_2} \end{bmatrix} \tag{2.9}$$

$$\boldsymbol{H}_i = \tilde{\boldsymbol{H}}_i \boldsymbol{\Phi}(t_i, t_k) \qquad \boldsymbol{\Phi}(t_i, t_k) = \text{diag}\left[\boldsymbol{\Phi}_1(t_i, t_k), \boldsymbol{\Phi}_2(t_i, t_k)\right] \in \mathbb{R}^{12 \times 12} \tag{2.10}$$

2.3. Estimation model

The aforementioned equations serve as the foundation for developing an estimator that provides an estimated state that best matches the measurement results [67]. These measurements do not have to represent the estimated states itself, but the observables are related to the states and dynamical model parameters. Besides measurements uncertainty, an important part related to the problem of AOD is the uncertainty of dynamic models. A traditional technique is to incorporate some dynamical model parameters as supplementary estimate parameters alongside the spacecraft states. The formal errors of the relevant parameters that come from this are thus indicative of the uncertainty induced by the dynamical model itself [73]. A filtering method is thus required to provide an approximation of the trajectory states and parameters used in the dynamic model [73, 74]. Measurement bias can also be estimated, which represents the uncertainty of the measurement model instead [20]. There is a variety of algorithms that can be used to correct the model states. These are divided into two main groups: sequential filtering and batch filtering [23, 75, 76]. Both methods are similar in that they aim to decrease the uncertainty linked to the estimated state and minimize the measurement error. The batch and sequential filtering techniques are discussed in Section 2.3.1 and Section 2.3.2 respectively.

2.3.1. Batch filtering

The batch filter processes an entire observation set at once, so it uses more than one observation before estimating the next state. BLS are mostly used for offline processing purposes, driven by operational scenarios in which data can only be downloaded within certain time windows (such as ground stations) [15]. The BLS has been applied to the context of AOD before [15, 46, 67]. The BLS filter offers the benefit of producing state estimates with lower error-covariance than sequential estimation filters [23]. Another benefit with respect to the sequential estimation techniques is that the batch filter is less susceptible to initial errors [75].

For each epoch in fit span $i = 1, \ldots, \ell$ the measurement residuals and STMs are calculated. The $\tilde{\boldsymbol{H}}_i$ matrices are converted into $\boldsymbol{H}_i$ using Equation 2.10. The observation-state relationship at t_i is mapped back to the epoch at the start of the measurement batch t_k [15]. The weighted least-squares estimate of the state vectors is computed by minimizing a cost function of the observation residuals, which are weighted by the random noise described by the respective observables, defined in $\boldsymbol{W}$. Errors are assumed to be independent [23]. The normal equation shown in Equation 2.11 yields this optimal result.

$$\delta\hat{\boldsymbol{x}}_k = \left(\boldsymbol{H}^T\boldsymbol{W}\boldsymbol{H}\right)^{-1}\boldsymbol{H}^T\boldsymbol{W}\delta\boldsymbol{y} = \boldsymbol{\Lambda}^{-1}\boldsymbol{N}\delta\boldsymbol{y} \tag{2.11}$$

The normal equation consists of the information matrix and information vector. This value is then used to adjust the initial state of the nominal state. An a-priori covariance matrix $\boldsymbol{P}_0$ could be added to the information matrix.

$$\begin{aligned} \boldsymbol{\Lambda} &= \boldsymbol{P}_0^{-1} + \boldsymbol{H}^T\boldsymbol{W}\boldsymbol{H} = \boldsymbol{P}_0^{-1} + \sum_{i=1}^{\ell}\boldsymbol{H}_i^T\boldsymbol{W}\boldsymbol{H}_i \\ \boldsymbol{N} &= \boldsymbol{H}^T\boldsymbol{W}\delta\boldsymbol{y} = \sum_{i=1}^{\ell}\boldsymbol{H}_i^T\boldsymbol{W}\delta\boldsymbol{y}_i \end{aligned} \tag{2.12}$$

2.3.2. Sequential filtering

The sequential filters, on the other hand, analyze the data one observation at a time, and update their state estimates real-time depending on the newly provided observations. The state uncertainty is known at each epoch which provides a real-time understanding of how fast and how accurate navigation is performed [15].

Extended Kalman Filter

A common way to combine the states of the dynamical model with the measurements is to use a sequential filter like the Extended Kalman Filter (EKF), an adaption of the linear Kalman Filter (LKF) that requires a linearization of a non-linear dynamics and measurement equations [75].

$$\begin{aligned}
\delta\bar{\boldsymbol{x}}_k &= \boldsymbol{\Phi}\left(t_k, t_{k-1}\right)\delta\hat{\boldsymbol{x}}_{k-1} \\
\bar{\boldsymbol{P}}_k &= \boldsymbol{\Phi}\left(t_k, t_{k-1}\right)\boldsymbol{P}_{k-1}\boldsymbol{\Phi}^T\left(t_k, t_{k-1}\right) + \boldsymbol{Q} \\
\boldsymbol{K}_k &= \bar{\boldsymbol{P}}_k\tilde{\boldsymbol{H}}_k^T\left[\tilde{\boldsymbol{H}}_k\bar{\boldsymbol{P}}_k\tilde{\boldsymbol{H}}_k^T + \boldsymbol{R}_k\right]^{-1} \\
\delta\hat{\boldsymbol{x}}_k &= \delta\bar{\boldsymbol{x}}_k + \boldsymbol{K}_k\left[\boldsymbol{y}_k - \tilde{\boldsymbol{H}}_k\bar{\boldsymbol{x}}_k\right] \\
\boldsymbol{P}_k &= \left[\boldsymbol{I} - \boldsymbol{K}_k\tilde{\boldsymbol{H}}_k\right]\bar{\boldsymbol{P}}_k\left[\boldsymbol{I} - \boldsymbol{K}_k\tilde{\boldsymbol{H}}_k\right]^T + \boldsymbol{K}_k\boldsymbol{R}_k\boldsymbol{K}_k^T
\end{aligned} \tag{2.13}$$

To avoid filter saturation, the state noise compensation matrix $\boldsymbol{Q}$ is introduced to the time update step in Equation 2.13 [13]. This matrix is used to adjust for unmodeled accelerations and prevent the filter from becoming unresponsive to later data [52]. The matrix is different for different sources [67, 13, 19]. The version used in this work will be that of Hill [13].

There exist a variety of adaptions on the EKF. The EKF is heavily influenced by poorly predicted values for components in the process noise matrix which might lead to low performance of the EKF [77]. For example, the Adaptive Extended Kalman Filter (AEKF) aims to improve the filter performances by adaptively estimating $\boldsymbol{Q}$ and $\boldsymbol{R}$ based on innovation and residual [77]. In order to counter the effects of inaccurate $\boldsymbol{P}_0$, the square root and fading filter EKF are invented [57].

Consider Kalman Filter

The precision with which the dynamics and measurements are described determines the performance of the estimate filters. Discrepancies in assumptions on force/measurement model such as simplifications and statistical parameters of assigned random errors, but also numerical round-off and truncation errors, can lead to an enlarged uncertainty of the states [23]. Consider covariance analysis is used to evaluate the effect of the exclusion of unknown or poorly known model parameters on the state uncertainty. The Consider-Kalman Filter (CKF) can be utilized for this [78, 6, 75]. It is predicated on an a priori estimate and the accompanying covariance matrix. The CKF differs somewhat from the EKF in that it involves the implementation of a consider parameter $\boldsymbol{b}_k$, and bias covariance matrix, $\boldsymbol{B}_0$, both of which must be included in the prediction step [75].

Prediction step

$$\bar{\boldsymbol{C}}_k = \boldsymbol{\Phi}\left(t_k, t_{k-1}\right)\boldsymbol{C}_{k-1} \tag{2.14}$$

Correction step

$$\begin{aligned}
\boldsymbol{K}_k &= \left[\bar{\boldsymbol{P}}_k\bar{\boldsymbol{H}}_k^T + \bar{\boldsymbol{C}}_k\boldsymbol{N}_k^T\right]\boldsymbol{\Omega}_k^{-1} \\
\hat{\boldsymbol{x}}_k &= \boldsymbol{x}_k + \boldsymbol{K}_k\left[\boldsymbol{y}_k - \bar{\boldsymbol{H}}_k\boldsymbol{x}_k - \boldsymbol{N}_k\boldsymbol{B}_0\right] \\
\boldsymbol{P}_k &= \left[\boldsymbol{I} - \boldsymbol{K}_k\bar{\boldsymbol{H}}_k\right]\bar{\boldsymbol{P}}_k - \boldsymbol{K}_k\boldsymbol{\Omega}_k\bar{\boldsymbol{C}}_k^T \\
\boldsymbol{C}_k &= \bar{\boldsymbol{C}}_k - \boldsymbol{K}_k\left[\boldsymbol{H}_k\bar{\boldsymbol{C}}_k + \boldsymbol{N}_k\boldsymbol{B}_0\right] \\
\boldsymbol{\Omega}_k &= \bar{\boldsymbol{H}}_k\bar{\boldsymbol{P}}_k\bar{\boldsymbol{H}}_k^T + \boldsymbol{N}_k\bar{\boldsymbol{C}}_k^T\bar{\boldsymbol{H}}_k^T + \bar{\boldsymbol{H}}_k\bar{\boldsymbol{C}}_k\boldsymbol{N}_k^T + \boldsymbol{N}_k\boldsymbol{B}_0\boldsymbol{N}_k^T + \boldsymbol{W}_k
\end{aligned} \tag{2.15}$$

Unscented Kalman Filter
Another option is the Unscented Kalman Filter (UKF) [79]. While the EKF filter requires a linearization of the non-linear dynamics, the UFK does not require linearized dynamics and can thus operate on a non-linear problem directly. This can be useful then the linearization assumptions are not valid [79, 67, 75]. This comes at a computational cost but it also improves in accuracy as linearization errors are not there anymore. A downside of non-linear estimators is that changes in the predicted state might cause a deviation from the true trajectory caused by the non-linear nature of the dynamics [23, 75].

Sequential Least Squares
In addition to Kalman filtering, there are sequential filtering approaches based on least squares principles, such as Recursive Least Squares (RLS) and Least Mean Squares (LMS). RLS iteratively adjusts the state predictions by minimizing the sum of squared errors, whereas LMS iteratively updates state estimates using stochastic gradient descent optimization. The assumptions and computational complexity of Kalman filtering and RLS vary.

Particle filter
Sequential Monte Carlo (SMC) techniques or particle filters (PF) were developed to improve state accuracy, particularly in the case of non-Gaussian noise and multimodality. It works by providing particles that each have a certain probability of being the true state. As the dynamic model propagates, the likelihood of the particle locations is weighted. PF can suffer from the problem of particle degeneracy where a few particles dominate the distribution, leading to decreased particle diversity. Resampling is then performed to select a new set of particles for the next iteration to maintain diversity in the particle set. A downside is the PF is that is prone to inaccuracies as the state dimensions increase, also known as the curse of dimensionality.

Filter Type	Advantages	Disadvantages
Sequential		
Linear Kalman (LKF)	Efficient and optimal for linear systems with Gaussian noise.	Only works for unimodal linear systems with Gaussian noise.
Extended Kalman (EKF)	Handles non-linear systems, can be used for non-linear estimation problems.	Can be sensitive to strong non-linearities and non-Gaussian noise.
Unscented Kalman (UKF)	Handles non-linear, continuous, multivariate problems.	Not multimodal, may not handle occlusions well, does not handle strongly non-Gaussian noise or very non-linear problems as well.
Recursive Least Squares (RLS)	Good at tracking time-varying parameters, can handle non-stationary processes.	More computationally expensive than other filters, requires more memory to store previous observations.
Least Mean Squares (LMS)	Good for adaptive filtering and can converge to the true filter coefficients.	Can be sensitive to initialization and can have slow convergence.
Particle Filter (PF)	Can handle multimodal distributions and non-Gaussian noise, flexible and versatile.	Requires large particle count for good performance, falls short at very high-dimensional systems.
Batch		
Batch Least Squares (BLS)	Simple to implement and computationally efficient when applied to large datasets.	Cannot be used for real-time filtering, may not handle time-varying parameters as well as sequential filters.

Table 2.1: Key characteristics of different filtering techniques. Sources: [80, 76, 23, 75]

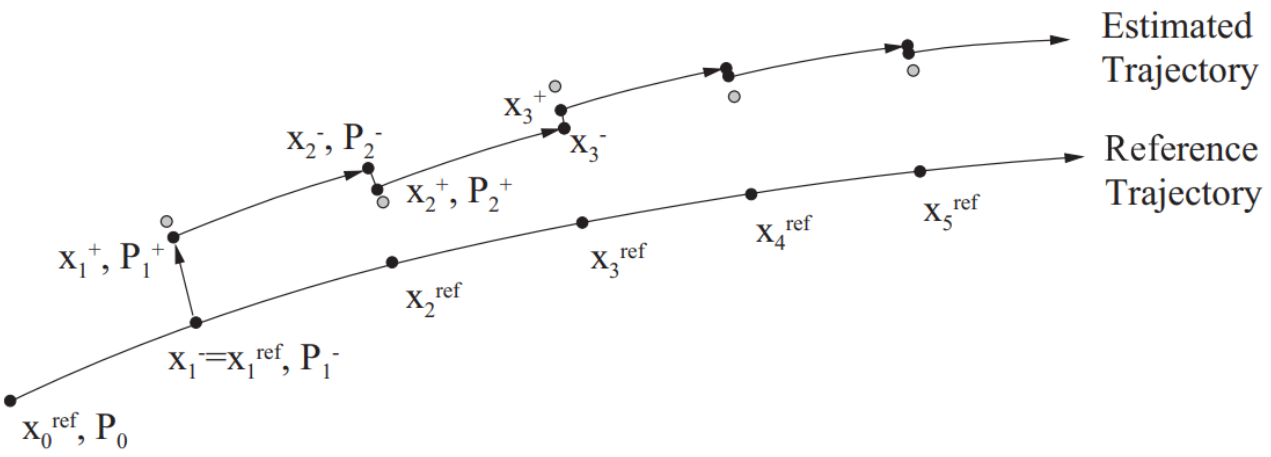

Figure 2.1: Linear Kalman filter. Source: [75]

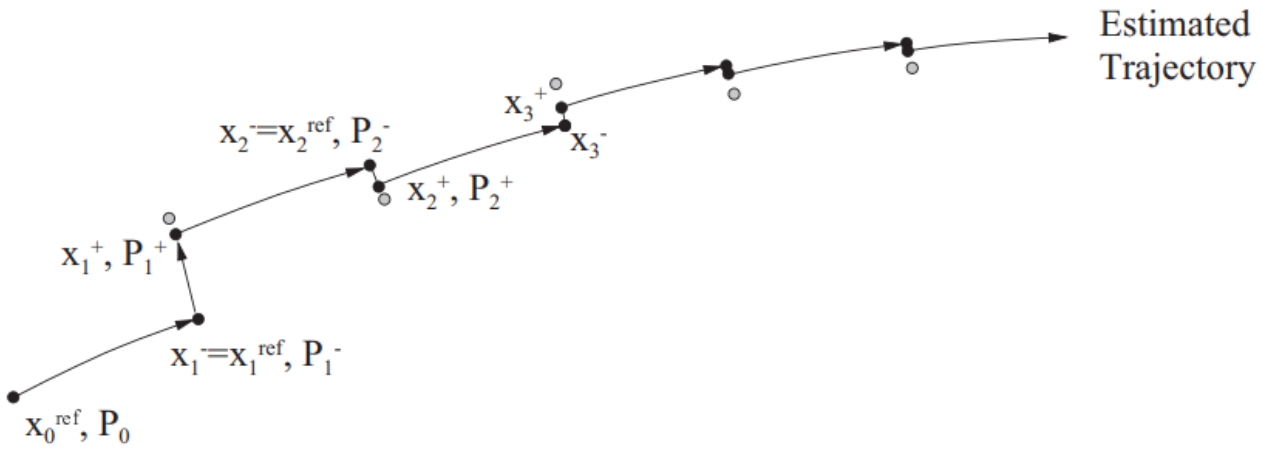

Figure 2.2: Extended Kalman filter. Source: [75]

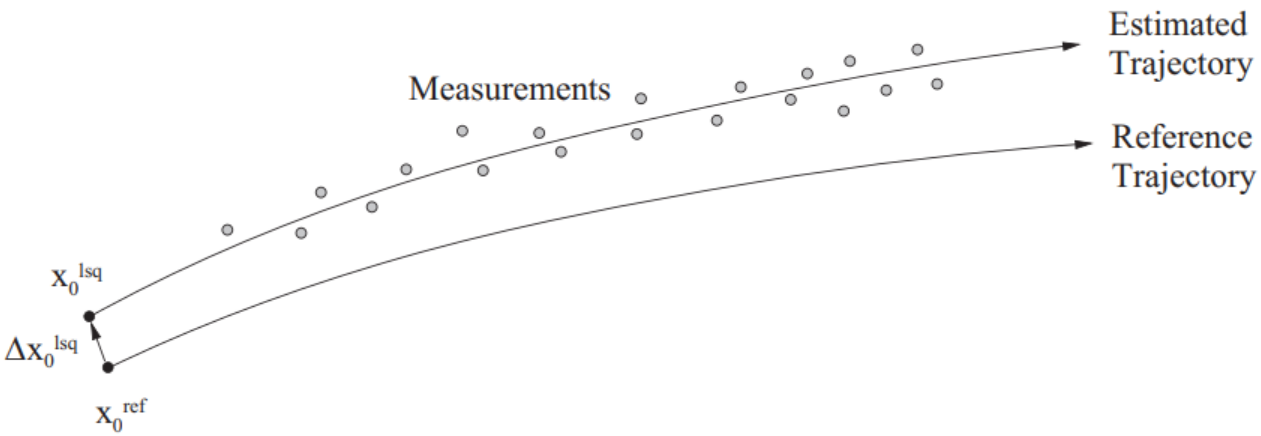

Figure 2.3: Batch Least Squares filter. Source: [75]

2.4. Observability

In the context of OD, observability refers to its capacity to acquire a unique estimation of a spacecraft's states [23, 42]. An increase in observability is correlated to the accuracy of state knowledge and is used when one wants to relate OD performance to the relative spacecraft geometry, measurement type, accuracy, measurement frequency [15]. Each new sensor observation adds new information to the system and thereby increases the observability [81]. The effectiveness of these measurements are a result of the geometric diversity of the orbit trajectories [61]. The degree to which radiometric measurements provide information on the states can be derived from eigenvectors and eigenvalues resulting from the information matrix or "Observability Gramian" $\mathbf{\Lambda}$ as shown in Equation 2.16. It represents the sum of "observation effectiveness" elements $\delta\mathbf{\Lambda}\left(t_i\right)$ at observation $i = 1, \dots \ell$ with $\delta\mathbf{\Lambda}\left(t_i\right) \in \mathbb{R}^{12\times12}$ [15] It essentially represents the sensitivity of a observable type to the initial conditions of the system [61].

$$\mathbf{\Lambda} = \sum_{i=1}^{\ell} \delta\mathbf{\Lambda}\left(t_i\right) = \sum_{i=1}^{\ell} \boldsymbol{H}_i^T \boldsymbol{W} \boldsymbol{H}_i = \sum_{i=1}^{\ell} \mathbf{\Phi}^T\left(t_i, t_0\right) \tilde{\boldsymbol{H}}_i^T \boldsymbol{W} \tilde{\boldsymbol{H}}_i \mathbf{\Phi}\left(t_i, t_0\right) \tag{2.16}$$

A property of $\mathbf{\Lambda}$ is that its inverse is the covariance matrix $\boldsymbol{P}$. With a known a priori $\boldsymbol{P}_0$, observability and covariance can be related. For measuring total observability, one should ignore $\boldsymbol{P}_0$ as it tends to give a warped image of the true value as one has to guess the initial value [15].

$$\mathbf{\Lambda} = \boldsymbol{P}_0^{-1} + \sum_{k=1}^{\ell} \boldsymbol{H}_i^T \boldsymbol{W} \boldsymbol{H}_i \tag{2.17}$$

When determining observability, the batch processor is very helpful, but it is difficult to predict how the covariance matrix would change when processing observations in real time [23]. A sequential filter shows how much measurements one needs to get to a good orbit estimate and how the covariance matrix changes at a moment in time. If the information matrix has full rank, one can observe all position and velocity states [8].However, full rank does not assess the magnitude of observability [81]. The order of observability depends on factors such as relative orbit geometry, constellation satellite count and measurement type [42, 41]. $\mathbf{\Lambda}$ can be split into an element related to the position states of spacecraft 1 and 2, leading to $\delta\mathbf{\Lambda}_1 \in \mathbb{R}^{3\times3}$ and $\delta\mathbf{\Lambda}_2 \in \mathbb{R}^{3\times3}$ respectively [15]. The effectiveness of the measurement for a particular position state is the eigenvalue belonging to the eigenvector of the respective state. The norms of the eigenvectors derived from $\mathbf{\Lambda}$ are an indication of the amount of useful information gathered from an observation of a particular state. For that, $\mathbf{\Lambda}$ has to be positive definite [15]. The maximum of observability effectiveness of the position vectors can be described by Equation 2.18 [15]. Symbol i refers to the columns of $\delta\mathbf{\Lambda}$.

$$\sqrt{max||eig(\delta\boldsymbol{\Lambda_i})||} \qquad i \in 1, 2, 3 \tag{2.18}$$

How state uncertainty changes over time is defined by the $\mathbf{\Phi}\mathbf{\Phi}^T$ matrix. Integration of the STM in the case when a nominal trajectory is periodic gives the monodromy matrix and gives special eigenvalue properties [15, 66]. The last two of its six eigenvalues indicate the stable and unstable manifolds or, in other words, the principle axis in the ellipsoid that have $||\lambda|| \leq 1$ and $||\lambda|| > 1$ respectively [82]. If the STM is propagated over other time scales than one orbit period, one obtains "local" manifolds. An unstable manifold refers to the direction in the error ellipsoid in which state uncertainty builds up over time. A more effective observation senses along the wide axis of the uncertainty ellipsoid. The more perpendicular the observations are with respect to the unstable manifold, the worse the observation effectiveness. This can be seen by the timing and extent of "blackout periods" over time by K. A. Hill [15]. Since the observation direction with respect to the error ellipsoid matters, it means that measurement effectiveness depends on the relative orbit geometries of the two satellites performing SST. Plotting observability provides insight into an optimal timing observation strategy while taking into account the limitations of the sensors onboard. The moments at which the eigenvalues of the information matrix are the largest could be the best moments to perform observations [83]. The observability can also be applied to parameters that are used in the dynamical system [83].

From the eigenvectors derived from the monodromy matrix one can also find the "sensitivity", a slightly different metric but seems to refer to the same idea as state above [30, 64].

$$S = \frac{1}{2}\left(||\lambda_i|| + \frac{1}{||\lambda_i||}\right) \tag{2.19}$$

In Equation 2.19, one uses the eigenvalues from the monodromy matrix associated with the (un)stable subspace of the orbit. In case an orbit is stable or unstable, one has $S \leq 1$ and $S > 1$ respectively [64]. Another way to quantify the degree of observability is by the condition number. This is defined as the ratio of the largest to the smallest eigenvalue of the information matrix. A smaller condition number represents better observability [61]. The system is considered not observable if the condition number is larger than 10^{16} [84].

2.4.1. Previous observability research

Most observability analyses have been performed based on orbits around the Earth in the context of formation flying. These were based on angle-only [81, 85, 86, 41, 87], angle and angle-rate [83] or range-only [51, 42, 88, 89] measurements. For such two body systems, only local observability can be achieved without additional predefined knowledge on the system because these two body problems provide more than one solution for a set of measurements [89]. More importantly, cislunar formations with LPO's were conducted as well, although to a lesser extend [15, 6, 61]. The amount of information acquired at a certain epoch can be seen in Figure 2.4 and Figure 2.5.

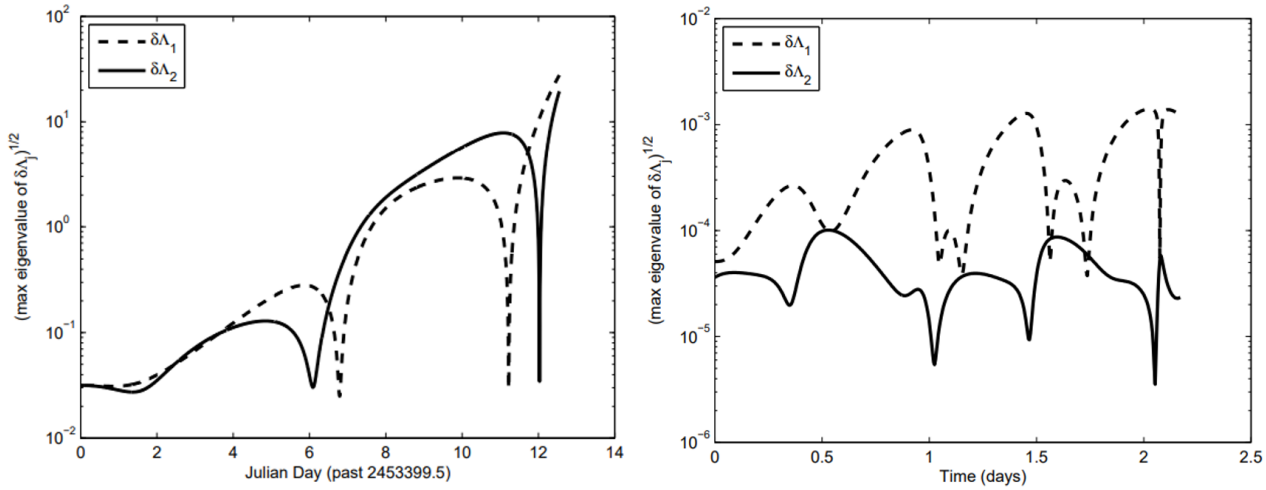

Figure 2.4: Observation effectiveness for two different orbit combinations. Source: [15]

Another example of the time change of observability can be seen in the research done on the LUMIO/LPF mission by Turan et al [6]. Again, the blackout periods can be observed from which optimal tracking windows can be derived.

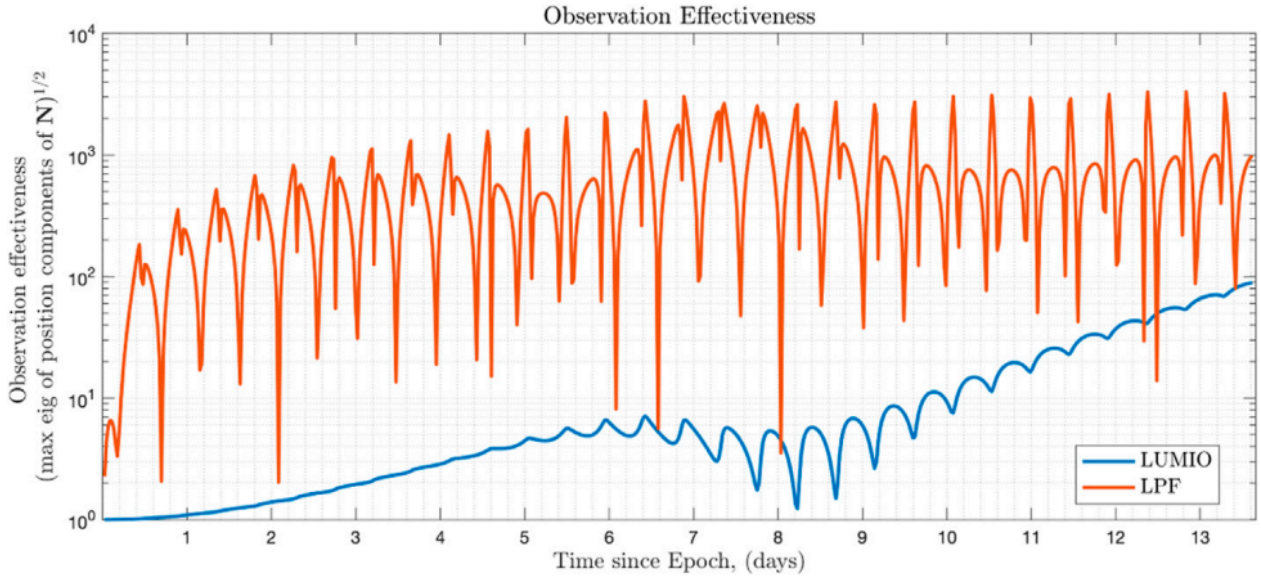

Figure 2.5: Observation effectiveness of the LUMIO-LPF constellation. Source: [6]

2.4.2. Observability adjusted estimation filters

In the non-linear system, the amplitude of the observability degree varies as the state changes, which has a significant relationship to the accuracy obtained from estimation filters [42]. There are also so-called observability-based filters: modified extended Kalman filter (MEKF), modified unscented Kalman filter (MUKF), and modified state-dependent Riccati equation filter (MSDREF). These change the error covariance matrix based on the observability of the system. This has been shown to enhance accuracy over the traditional counterparts, but only position states were examined and the simulated environment included two LEO satellites [42]. The vastly different geometries of the LUMIO-LPF scenario might yield different conclusions. The SDREF does not need linearization to approximate a dynamic model and measurement model, and it does not need the Jacobian for the STM used in state covariance matrix prediction. As a consequence, in a comparable circumstance with two formation flying LEO spacecraft, the SDREF has demonstrated to have a lower computational burden than the EKF while simultaneously enhancing accuracy [90]. The SDREF does not handle non-linear noise and a adaption, the SDREF/PF, was built by Chang et al [91]. It was shown here that SDREF/PF is less sensitive to changes in measurement noise covariance $\boldsymbol{R}$ and converges faster than the SDREF, UKF and PF in the case of estimating the states of the Rössler attractor.

2.5. Uncertainly propagation

Ideally, measurements of the true spacecraft state are done at a very high frequency. However, this might not always be possible or necessary. To obtain an estimation of the probability density of the possible states for epochs after the last measurement, one needs to propagate the statistical moments of this distribution over time. The values of these moments depend on the errors included in the measurement and dynamical models [23]. If there are no errors in the dynamical model, noise and bias that occur throughout the measurement process are the only cause of errors between model and actual state values [65]. Not including models parameters in the estimation leads to an overly-optimistic noise-only covariance matrix time evolution and does not represent a realistic uncertainty envelope anymore [73, 74]. In the non-ideal case, dynamical model errors can be split up into the categories of aleatory and epistemic errors [92, 65].

- **Epistemic errors**
  Errors caused by a slight misrepresentation of the true accelerations in the acceleration model, i.e. to save on computer memory and processing time. Numerical solution techniques, such as discretization and approximation errors, and convergence precision, are also considered epistemic errors.
- **Aleatory errors**
  Errors that arise from the inherent stochastic nature of reality. If there were no epistemic errors, there would still be some random errors between expectation and reality.

In general, the uncertainties are believed Gaussian and independent, as this makes to possible to describe the distribution of the state by just the first two statistical moments, so mean and covariance [65]. There exist a variety of techniques to quantify the state uncertainty. Three commonly used techniques are explained below.

- **Monte Carlo**
  An intuitive solution which works on non-linear systems and with Gaussian uncertainties [65]. This method randomly generates initial state errors, propagates the dynamics and creates an empirical distribution, and thus mean and variance of the states. The statistics may only be generated for one epoch and lead to a large computational burden [59, 65].
- **LinCov analysis**
  Another option which requires a linearization the system [26, 65]. This can be done under the assumptions that

  1. A linearized model approximates the dynamics of nearby trajectories sufficiently with regard to a nominal trajectory (the STM from Section 2.1 is used for this)
  2. A Gaussian probability distribution can properly capture the uncertainty [65].

  Estimating the time span over which Linear covariance (LinCov) can be used is then based on of knowledge of when the Gaussianiaty assumption breaks [17]. Additionally, since non-linear uncertainty propagation methods demand a greater amount of processing power than linear propagation methods, estimating the time when the Gaussianity of the uncertainty breaks is critical for obtaining optimal computational effectiveness [17]. Multiple approaches exist to determine when this happens, such as the Henze-Zirkler

test for multivariate normality (MVN) or the Unscented transform based normalized offset (UNO) [93]. This method is computationally much more efficient and can be used in autonomous onboard mission planning [94, 95]. However, with the linearized system it becomes challenging to obtain the uncertainty from the orbit when the spacecraft is in an unstable environment or when evaluated over a relatively long time frame [59].

- **State Transition Tensors**
  A higher-order version of the STM where its terms can be added to the linearized version of LinCov as a extension of the Taylor series. Non-linear factors that are overlooked during the linearization process might have a significant impact on the solution's correctness [96]. In order to effectively explain uncertainty, the State Transition Tensors (STTs) account for non-linearities in the propagation of the mean and covariance [96, 18, 59]. More accurate information regarding the real trajectory can contribute to a faster state estimation convergence [59]. This can be done by means of an adapted version of the EKF: Higher-Order Numerical Extended Kalman Filter (HNEKF) [65, 97].

  Benefits include:

  1. The STTs are costly to compute. However, once the STT history for a particular reference trajectory is obtained, the result is algebraically evaluated onboard to forecast the influence of any state deviation, removing onboard integrations. This advantage may result in a decrease in the need for ground station links for navigation purposes.
  2. Faster on-board computations for station-keeping maneuvers. It enables near-real-time trajectory planning in response to navigation errors, or other unanticipated events.
  3. Because nonlinear dynamics are more easily captured, the state departure from a reference orbit is more precisely known. As a result, the region of convergence for these approaches should be bigger than when only the first term is used.

  Overall, the STT approach outperforms others in terms of computational burden versus accuracy [98, 99]. Under impulsive maneuvers, an adapted version of the STT is used in the covariance analysis [99].

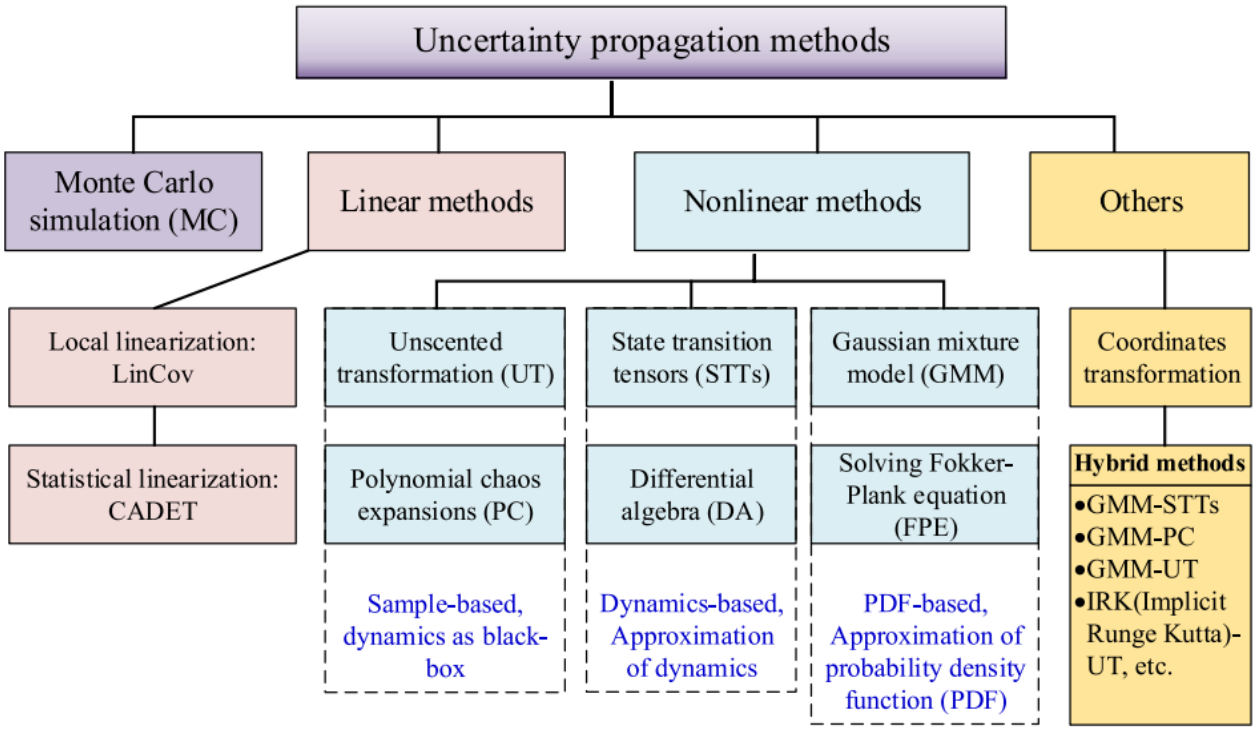

Figure 2.6: Illustration of different uncertainty propagation methods. Source: [65]

With a better knowledge of uncertainty development, one could establish tracking approaches that minimize the number of observations necessary to tighten the uncertainty envelope [100]. An important aspect

to note is that some dynamical regimes other than two-body periodic dynamics, like libration point orbits and near-rectilinear orbits, require adaptations to the standard STT method for accuracy and time improvements [101].

2.6. Comparing dynamical models

As discussed in Section 2.1, the number of bodies included in the model influences the degree to which the ”real” dynamics are calculated. The following two main aspects are important to keep in mind when working with those different models:

- **Model assumptions**
  The CRTBP assumes circular orbits and neglects various perturbations such as atmospheric drag, solar radiation pressure, and the gravity of celestial bodies. From Section 2.4 and Section 2.5 one notices that STMs and STTs are used and signify measurement weak points. These model assumptions might not provide the most realistic image of the dynamics and thus distort the STMs and STTs and thus the true error and observability values over time, which influences the planning of when new measurements should be taken. It is preferred to be able to simulate the error propagation over a period of longer than 14 days and the CRTBP might diverge quickly from the planned trajectory than the high-fidelity model.
- **Computational efficiency**
  Because of its simplified structure, the CRTBP is less computationally expensive than a high-fidelity dynamical model. Considering again the error propagation, it might be that CRTBP eventually maybe lead to more computational cost and complexity because of more required measurements.

One could assess the trade-off between computing efficiency and accuracy by comparing the two models. This comparison can aid in determining the best model for a specific scenario by balancing the demand for accuracy with the computing resources available. One should keep in mind that having the most optimal solution is not as crucial as having a practical one. It is critical to grasp the benefits and drawbacks of the solutions. From an operational perspective, the best and worst solutions can establish a distinct envelope of possible timings that might not provide the best state accuracy, but is sufficient for the mission. The assumptions used in the model will likely influence the state uncertainty over time. Questions arise such as what range of timing and at what moment in orbit are measurements preferred? At what point or range in time or orbit does one say that a missed session leads to unacceptable errors? Is there an optimal quantity of measurements depending on time and location? What level of uncertainty is considered too much? This could be beneficial because future much missions need to work with a flexible schedule because, for example, the relay satellite also has its own scheduling and might be preoccupied by communicating with other satellites in the future and lunar occultations can occur [3].

2.6.1. Result validation procedures

This work aims to produce its own models to perform calculations, but one should also be able to validate the models by means of independently produced simulation results. Politecnico di Milano has produced results that are the result of an optimized CRBTP orbit in the n-body problem with the objective of minimizing ΔV as done similarly by the EQUULEUS mission [2]. The data is given for the full 1-year operational orbit between 21 March 2024 and 21 March 2025. In order to compare the validation data and the models, one has to compare the coordinates defined with respect to the same reference system. For the low-fidelity CRTBP model, one has to convert the non-dimensionalized Earth-Moon rotational barycentric coordinates of the CRTBP to the Earth-centered body-fixed frame [6, 102]. One also has to take into account the precession and nutation effects of the earth at the specified epochs. The CRTBP can be made in two ways: with the approach in Section 2.1.1 or using Tudat. The Tudat states should be validated by comparing it with the trajectories obtained by Turan et al. [6].

3

Potential research contribution

This chapter aims to provide an overview of possible research topics to improve the current body of knowledge of AOD in cislunar space. Broadly speaking, it will be focused on the aspect of the timing of satellite-to-satellite links by providing an envelope of SST possibilities in orbital position and time that makes sense from an operational perspective.

- **Tracking timing based on observability information**
  From the found literature the OD measurements are assumed to take place at a certain frequency [15, 34]. From an operational and technical perspective, this constant connection with the other satellite might not be feasible. In Section 2.4 it was stated that there exist blackout periods that influence the effectiveness of the OD. Knowledge on when those periods occur can be used to concentrate measurements at a greater frequency or overall duration. Because once such a blackout occurs, the most beneficial observations are effectively lost and better moments in time could have been utilized. Optimized windows for observation can result in lower propellant consumption, easier mission operations, and longer mission times. Grouping tracking windows, however, can also assist in lowering the total cost of navigation by lowering the setup operations associated with tracking, such as antenna pointing [20].
- **Autonomous navigation assessment for more than 14 days**
  Turan et al. [6] simulated the orbit determination of LUMIO-LPF over one LUMIO period of 14 days. This work does not provide a full insight of the fully autonomous behavior of the LPF-LUMIO system over the planned 1 year mission duration. The process of OD, uncertainty propagation and station keeping are all connected but not brought into one coherent picture. The S/K maneuvers of LUMIO are currently conducted in the (7, 7, 14) days pattern (using the TPM). Strategies should be implemented to assess the effect of adjusting tracking windows. Without ground station planning, tracking and S/K strategies could be adjusted, while still taking into account constraints on availability between satellites due to ongoing science operational priorities [26, 3], power and accuracy requirements [103, 6], body occultations [3], etc. The timing of SST sessions could allow for increased state accuracy and thereby alter S/K strategies and ΔV [40]. The effect of S/K maneuvers on LiAISON's performance was recommended in literature [5]. The effect of semaphores could be implemented to assess the effect of omitted/shifted/shorted/elongated tracking windows.
- **Improved fidelity of the dynamical model**
  An aspect to consider is that most research was done based on the CRTBP. K. A. Hill [15] did an extensive analysis by comparing a large range of orbit combinations using CRTBP. A high-fidelity environment might give a more accurate description of the dynamics which can allow for a smaller error between the predetermined orbit and actual orbit after OD sessions. This might lead to the option to start and/or end the estimation process later and earlier respectively.
- **Higher order state uncertainty propagation**
  In the estimation phase, the state error and covariance converges to smaller values over time. The opposite is true once the last measurement is conducted as the uncertainty of the position of the spacecraft increases again [41]. This uncertainty propagation is best done by the STT technique to capture the nonlinear effects as discussed in Section 2.5. This can be done for the states of both satellites separately.

The state deviation distribution could behave quite differently between the two spacecraft due to their different dynamical nature. State uncertainty knowledge provides information on what happens when a tracking session is missed. This then gives a sense of how much the estimation filter is expected to converge from.

- **Use of BLS and UKF estimation filter**
  The type of utilized estimation filter can improve the state estimation, which also results in an alteration of the state uncertainty. Most literature makes use of the EKF, but the UKF provides a full non-linear estimation. Additionally, the BLS is used for its easy implementation and availability within tudatpy.
- **Validation of Tudatpy**
  The state and STM histories obtained from tudatpy are used for all calculations of the observability analysis and estimation process and S/K corrections. For the low-fidelity model, the results of the tudatpy CRTBP equivalent and the true CRTBP can be compared.
- **Validity of EKF by checking Non-Gaussian uncertainties**
  The EKF is one of the most used estimation filters in literature. The primary assumption of the EKF is that the state estimates and uncertainties are Gaussian. Another way in which the timing of satellite links can be determined is by knowledge on the diverge from Gaussian to non-Gaussian uncertainty envelopes using statistical MVN tests. Knowledge on when this assumption breaks can give insight into when the EKF assumption becomes implausible to use for AOD.
- **Semaphores**
  One could also consider novel tricks such as using simple ultra-low rate signals (semaphores) to communicate basic needs. This way a satellite could quickly assess the status of the mission and serve it upon request. This should be done while still adhering to the requirements of the satellites shown in Table 1.1.

3.1. Research questions

Considering the current state-of-the-art, the thesis work will aim to conduct research concerning the following research objective and questions:

Research objective

"To investigate the ability to increase the accuracy of satellite autonomous navigation of existing LiAISON-based cislunar smallsat missions by scheduling satellite-to-satellite tracking sessions as efficiently as possible."

Main research question

"What is the most optimal satellite-to-satellite tracking timing strategy for LiAISON-based cislunar smallsat missions to increase navigation accuracy?"

Sub questions

1. What parameters influence the observability effectiveness of autonomous navigation observations?
2. What are the discrepancies in navigation accuracy between using the CRTBP and a high-fidelity model as the dynamical model?
3. What influence do estimation filter parameters have on the state accuracy?
4. What operational limitations exist that can affect the state accuracy?

3.2. Theoretical content/Methodology

This research work has the nature of a causal study and will follow deductive reasoning philosophy. This section will discuss the main steps that will be performed. The work will not include certain lab or field experiments, but aims to look at the extent to which there is a causal effect of the before mentioned parameters on

navigation accuracy. From a practical perspective, this work is close to the supervisor's work which allows for efficient cooperation and information exchange. Details might adjust over time. The goal will be to optimize the observation accuracies by minimizing the blackout periods in the effectivenesses plots, see Chapter 2. This is to remove the effectiveness dips and the overall magnitude as much as possible by means of adjusting a variety of variables shown in Chapter 3. Separate CTBRP and high-fidelity dynamical models are propagated using the same initial states. S/K methods from Section 2.1.4 will be used. As input for the estimation filter, the estimation model requires the initial states and the range measurements. The final accuracy results from a Monte-Carlo simulation to obtain a mean and confidence interval. A RMS value based on Monte-Carlo values calculated at each epoch determines the accuracy at a moment in time.

3.3. Expected results and outcomes

3.3.1. Results

The final results will be plots comparing initial and optimized observation effectiveness for position states. The state accuracy plots show the errors with 3σ over a time period of the mission lifetime, also for initial and improved results. A table or orbit plot will include an overview of the measurement time steps and the moment it occurs in orbit. The specific parameters from Chapter 3 will be put in a table. Verification and validation has to be performed as well. Because TU Delft has close ties with the LUMIO mission, the simulated dynamics of the LUMIO mission can be compared to the computed LUMIO states used by the LUMIO team, ranging from March 21st to April 4th of 2024. These states are considered the "true" states as these have been verified before. The research by Turan et al. [6] provides plots of the RMS accuracies of the states for LUMIO and the LPF. This can be used to verify the measurement and estimation model code. Since other cislunar missions seem to not openly provide such information it could be the case that mid-study the focus is put on the LUMIO mission only. Regarding S/K, the 3σ ΔV value is consistent with those from LUMIO [30]. Regarding data management, files will be stored privately on GitHub. The LUMIO state files are confidential. This will be shared only with the supervisor.

3.3.2. Outcomes

With the statements from Section 1.2 in mind, one could expect an overall decrease in blackout periods and increase in the accuracy plots. These periods will be due to a result of employing an OD window in the faster parts in orbit. A higher measurement frequency will be necessary at those regions. Accuracies will decrease again in non OD regions, but the slower dynamics lead to slower error propagations. The high-fidelity model will result in the best accuracies. The AEKF will result in a better positional estimation than EKF and lead to faster convergence. S/K likely should be performed outside of observation windows. AOD will likely reduce the measurement cut-off times required for ground processing and, probably, reduce the errors as propagation is not required, allowing the error to build up.

4

Conclusion

To accommodate the future challenges of navigating cislunar objects, literature has shown that autonomous orbit determination based on the LiAISON navigation techniques can provide promising state estimation. Various research was done on the effects of orbital geometry, measurement types and estimation filters. Calculations are most often based on simplified dynamics and estimation filtering techniques that require certain assumptions to work. Additionally, most research assumes a fixed frequency of observations and does not focus on mission practicalities. From an operational perspective, inter-satellite links might not require continuous communications. Moreover, links might not be possible in cases when certain scientific objectives have to be met, occultations occur. or power budgets have to be met.

Regarding dynamical models, it was found that simplifications are made that neglect additional accelerational perturbations, thereby not providing an adequate picture of the expected dynamics. This affects the trustworthiness of the error propagations as some effects are not considered in the STM, which is crucial for covariance and observability analysis as it can lead to sub-optimal estimates. These are tools that can be used to determine spots in-orbit where measurements improve state knowledge best.

It was found that most often sequential filters, specifically the EKF, were used. This this, however, prone to errors in initial guesses on the covariance matrix, it assumes a Gaussian and additive noise distribution and the linearization should be valid. Adaptations of the sequential filters exist that improve the converge to a result that are less prone to initial guesses (AEKF) and work on a fully non-linear dynamics and non-Gaussian noise (UKF). Observability-based options exist as well. While mostly sequential filters have been used in literature, the batch least squares filter (BLS) might provide benefit as it is less susceptible to initial errors and has the capability to smooth out measurements.

While optimal state accuracy and lowest uncertainty is ideal, lower observational rates might suffice. Situations could occur in which it proves sufficient to perform measurements at fixed points or time intervals, or variable frequencies within orbital regions. Practical aspects might also include the use of semaphores that might signal whether observations will be needed in the next round. Overall, there is a trade-off between state accuracy and operational efficiency. Finding this while including all above mentioned considerations will be the overarching objective for this thesis. The thesis will work with the orbits from the LPF-LUMIO constellation with ranging-only measurements, but might broaden to other orbit types if time allows.

References

[1] A. Cervone *et al.*, "LUMIO: A CubeSat for observing and characterizing micro-meteoroid impacts on the Lunar far side," en, *Acta Astronautica*, vol. 195, pp. 309–317, Jun. 2022, ISSN: 0094-5765. DOI: 10.1016/j.actaastro.2022.03.032.

[2] K. Kota *et al.*, "EQUULEUS Mission Analysis: Design of the Science Orbit Phase," in *International Symposium on Space Technology and Science 2017*, 2017.

[3] B. Cheetham *et al.*, "CAPSTONE: A Unique CubeSat Platform for a Navigation Demonstration in Cislunar Space," in *Ascend 2022*, American Institute of Aeronautics and Astronautics, 2022. DOI: 10.2514/6.2022-4382.

[4] Z. Towfic *et al.*, "Simulation and analysis of opportunistic MSPA for multiple cubesat deployments," in *SpaceOps Conference 2018*, American Institute of Aeronautics and Astronautics, May 2018. DOI: 10.2514/6.2018-2396.

[5] S. G. Hesar *et al.*, "Lunar far side surface navigation using Linked Autonomous Interplanetary Satellite Orbit Navigation (LiAISON)," en, *Acta Astronautica*, vol. 117, pp. 116–129, Dec. 2015, ISSN: 0094-5765. DOI: 10.1016/j.actaastro.2015.07.027.

[6] E. Turan *et al.*, "Autonomous Crosslink Radionavigation for a Lunar CubeSat Mission," *Frontiers in Space Technologies*, vol. 3, 2022, ISSN: 2673-5075. DOI: https://doi.org/10.3389/frspt.2022.919311.

[7] E. Turan *et al.*, "Autonomous Navigation Performance of Cislunar Orbits considering High Crosslink Measurement Errors," in *IEEE Aerospace Conference 2022*, ISSN: 1095-323X, Mar. 2022, pp. 1–11. DOI: 10.1109/AERO53065.2022.9843772.

[8] T. Qin *et al.*, "Relative Orbit Determination Using Only Intersatellite Range Measurements," *Journal of Guidance, Control, and Dynamics*, vol. 42, no. 3, pp. 703–710, Mar. 2019, ISSN: 0731-5090. DOI: 10.2514/1.G003819.

[9] P. Rocha Cachim *et al.*, "Autonomous orbit determination for satellite formations using relative sensing: Observability analysis and optimization," *Acta Astronautica*, vol. 200, pp. 301–315, Nov. 2022, ISSN: 0094-5765. DOI: 10.1016/j.actaastro.2022.08.009.

[10] A. Grenier *et al.*, "Positioning and Velocity Performance Levels for a Lunar Lander using a Dedicated Lunar Communication and Navigation System," en, *NAVIGATION: Journal of the Institute of Navigation*, vol. 69, no. 2, Jun. 2022, ISSN: 0028-1522, 2161-4296. DOI: 10.33012/navi.513.

[11] A. Pasquale *et al.*, "Cislunar distributed architectures for communication and navigation services of lunar assets," *Acta Astronautica*, vol. 199, pp. 345–354, Oct. 2022, ISSN: 0094-5765. DOI: 10.1016/j.actaastro.2022.06.004.

[12] E. Turan *et al.*, "Autonomous navigation for deep space small satellites: Scientific and technological advances," en, *Acta Astronautica*, vol. 193, pp. 56–74, Apr. 2022, ISSN: 0094-5765. DOI: 10.1016/j.actaastro.2021.12.030.

[13] K. A. Hill *et al.*, "Autonomous Orbit Determination from Lunar Halo Orbits Using Crosslink Range," *Journal of Spacecraft and Rockets*, vol. 45, no. 3, pp. 548–553, May 2008, ISSN: 0022-4650. DOI: 10.2514/1.32316.

[14] E. Turan *et al.*, "Performance analysis of crosslink radiometric measurement based autonomous orbit determination for cislunar small satellite formations," en, *Advances in Space Research*, Nov. 2022, ISSN: 0273-1177. DOI: 10.1016/j.asr.2022.11.032.

[15] K. A. Hill, "Autonomous navigation in libration point orbits," Ph.D. dissertation, University of Colorado Boulder, Jan. 2007.

[16] G. Sirbu *et al.*, "Fully Autonomous Orbit Determination and Synchronization for Satellite Navigation and Communication Systems in Halo Orbits," en, *Remote Sensing*, vol. 15, no. 5, p. 1173, Jan. 2023, ISSN: 2072-4292. DOI: 10.3390/rs15051173.

[17] M. Gupta, “Analysis of the Representation of Orbital Errors and Improvement of their Modelling,” M.S. thesis, Luleå University of Technology, Sep. 2018.

[18] A. Bani Younes *et al.*, “High-order uncertainity propagation using state transition tensor series,” *Advances in the Astronautical Sciences*, vol. 147, Jan. 2013.

[19] L. Zhang *et al.*, “A Universe Light House — Candidate Architectures of the Libration Point Satellite Navigation System,” en, *The Journal of Navigation*, vol. 67, no. 5, pp. 737–752, Sep. 2014, ISSN: 0373-4633, 1469-7785. DOI: 10.1017/S0373463314000137.

[20] E. Turan *et al.*, “Particle Swarm Optimization Based Tracking Window Planning for Cislunar Orbiters Performing Autonomous Radiometric Navigation: 74th International Astronautical Congress (IAC),” *Proceedings of the 74th International Astronautical Congress (IAC)*, 2023.

[21] M. Sweeting, “Modern Small Satellites-Changing the Economics of Space,” *Proceedings of the IEEE*, vol. 106, no. 3, pp. 343–361, Mar. 2018, ISSN: 1558-2256. DOI: 10.1109/JPROC.2018.2806218.

[22] A. Freeman, “Deep Space NanoSats - positioned for exponential growth,” en, Tech. Rep., May 2016, Type: dataset.

[23] B. Tapley *et al.*, *Statistical Orbit Determination*. Elsevier, Jan. 2004, ISBN: ISBN: 0-12-683630-2.

[24] A. M. Al-Saegh *et al.*, “Atmospheric Propagation Model for Satellite Communications,” en, in *MATLAB Applications for the Practical Engineer*, IntechOpen, Sep. 2014, ISBN: 9789535117193. DOI: 10.5772/58238.

[25] R. A. Carvalho, “Optimizing the Communication Capacity of a Ground Station Network,” en, *Journal of Aerospace Technology and Management*, vol. 11, e2319, May 2019, ISSN: 2175-9146. DOI: 10.5028/jatm.v11.1026.

[26] D. Davis *et al.*, “Orbit Maintenance and Navigation of Human Spacecraft at Cislunar Near Rectilinear Halo Orbits,” in *27th AAS/AIAA Space Flight Mechanics Meeting*, Feb. 2017.

[27] W. Wang *et al.*, “Joint navigation performance of distant retrograde orbits and cislunar orbits via LiAISON considering dynamic and clock model errors,” en, *Navigation: Journal of the Institute of Navigation*, vol. 66, no. 4, pp. 781–802, 2019, ISSN: 2161-4296. DOI: 10.1002/navi.340.

[28] D. Lujan *et al.*, “Earth–Moon L2 Quasi-Halo Orbit Family: Characteristics and Manifold Applications,” *Journal of Guidance, Control, and Dynamics*, vol. 45, no. 11, pp. 2029–2045, Nov. 2022, ISSN: 0731-5090. DOI: 10.2514/1.G006681.

[29] K. Hamera *et al.*, “An Evolvable Lunar Communication and Navigation Constellation Concept,” in *IEEE Aerospace Conference 2008*, ISSN: 1095-323X, Mar. 2008, pp. 1–20. DOI: 10.1109/AERO.2008.4526326.

[30] A. M. Cipriano *et al.*, “Orbit Design for LUMIO: The Lunar Meteoroid Impacts Observer,” *Frontiers in Astronomy and Space Sciences*, vol. 5, Sep. 2018, ISSN: 2296-987X. DOI: https://doi.org/10.3389/fspas.2018.00029.

[31] K. Oshima, “The use of vertical instability of l1 and l2 planar Lyapunov orbits for transfers from near rectilinear halo orbits to planar distant retrograde orbits in the Earth–Moon system,” en, *Celestial Mechanics and Dynamical Astronomy*, vol. 131, no. 3, p. 14, Mar. 2019, ISSN: 1572-9478. DOI: 10.1007/s10569-019-9892-6.

[32] E. Turan *et al.*, “Performance Analysis of Radiometric Autonomous Navigation for Lunar Satellite Network Topologies: 11th International Workshop on Satellite Constellations and Formation Flying,” English, 11th International Workshop on Satellite Constellations and Formation Flying„ IWSCFF2022 ; Conference date: 07-06-2022 Through 08-06-2022, 2022.

[33] R. M. Suggs *et al.*, “The flux of kilogram-sized meteoroids from lunar impact monitoring,” en, *Icarus*, vol. 238, pp. 23–36, Aug. 2014, ISSN: 0019-1035. DOI: 10.1016/j.icarus.2014.04.032.

[34] T. Tanis, “Autonomous Orbit Determination in Cislunar Space,” en, M.S. thesis, Delft University of Technology, Aug. 2022.

[35] K. De Smaele, “Design of an Unsupervised Machine Learning Approach to Fault Detection for CubeSat AOCS: Applied to LUMIO: Lunar Meteoroid Impact Observer,” en, M.S. thesis, Delft University of Technology, May 2023.

[36] F. Nett, “On the Design of a Propulsion System for the Lunar Meteoroid Impact Observer (LUMIO),” en, M.S. thesis, Delft University of Technology, Oct. 2021.

[37] S. Gelmi, “Fault Detection Isolation and Recovery for LUMIO mission: Algorithm and Methodology,” en, M.S. thesis, Delft University of Technology, Sep. 2019.

[38] A. do Carmo Cipriano, “Orbit Design of a Lunar Meteoroid Impact Flashes Observer,” en, M.S. thesis, Delft University of Technology, Nov. 2017.

[39] S. Sirani, “Lumio orbit refinement in high fidelity model,” M.S. thesis, Politecnico di Milano, Dec. 2021.

[40] Y. Jin *et al.*, “A Modified Targeting Strategy for Station-Keeping of Libration Point Orbits in the Real Earth-Moon System,” en, *International Journal of Aerospace Engineering*, vol. 2019, e3257514, Sep. 2019, ISSN: 1687-5966. DOI: 10.1155/2019/3257514.

[41] Y. Hu *et al.*, “Three-spacecraft autonomous orbit determination and observability analysis with inertial angles-only measurements,” en, *Acta Astronautica*, vol. 170, pp. 106–121, May 2020, ISSN: 0094-5765. DOI: 10.1016/j.actaastro.2020.01.005.

[42] Y. Li *et al.*, “Observability analysis and autonomous navigation for two satellites with relative position measurements,” en, *Acta Astronautica*, Fourth IAA Conference on Dynamics and Control of Space Systems (DYCOSS2018), vol. 163, pp. 77–86, Oct. 2019, ISSN: 0094-5765. DOI: 10.1016/j.actaastro.2019.02.030.

[43] S. Damico *et al.*, “Autonomous formation flying based on GPS - PRISMA flight results,” English, *Acta Astronautica*, vol. 82, no. 1, pp. 69–79, 2013, ISSN: 0094-5765. DOI: 10.1016/j.actaastro.2012.04.033.

[44] K. Xiong *et al.*, “Autonomous navigation for a group of satellites with star sensors and inter-satellite links,” English, *Acta Astronautica*, vol. 86, pp. 10–23, 2013, ISSN: 0094-5765. DOI: 10.1016/j.actaastro.2012.12.001.

[45] S. Hur-Diaz *et al.*, “Autonomous lunar orbit navigation using optical sensors,” *Astrodynamics 2007 - Advances in the Astronautical Sciences, Proceedings of the AAS/AIAA Astrodynamics Specialist Conference*, Advances in the Astronautical Sciences, pp. 997–1014, 2008, ISSN: 9780877035435.

[46] M. B. Hinga *et al.*, “Autonomous Lunar L1 Halo Orbit Navigation Using Optical Measurements to a Lunar Landmark,” en, *NAVIGATION: Journal of the Institute of Navigation*, vol. 70, no. 3, Sep. 2023, ISSN: 0028-1522, 2161-4296. DOI: 10.33012/navi.586.

[47] N. Bradley *et al.*, “Cislunar Navigation Accuracy Using Optical Observations of Natural and Artificial Targets,” *Journal of Spacecraft and Rockets*, vol. 57, no. 4, pp. 777–792, Jul. 2020, ISSN: 0022-4650. DOI: 10.2514/1.A34694.

[48] C. D. Murray *et al.*, *Solar System Dynamics*. Cambridge: Cambridge University Press, 2000, ISBN: 9780521575973. DOI: 10.1017/CBO9781139174817.

[49] S. Mo *et al.*, “Multi-Satellite Relative Navigation Scheme for Microsatellites Using Inter-Satellite Radio Frequency Measurements,” *Sensors (Basel, Switzerland)*, vol. 21, no. 11, p. 3725, May 2021, ISSN: 1424-8220. DOI: 10.3390/s21113725.

[50] A. Genova *et al.*, “Deep-Space Navigation with Intersatellite Radio Tracking,” *Journal of Guidance, Control, and Dynamics*, vol. 44, no. 5, pp. 1068–1079, May 2021, ISSN: 0731-5090. DOI: 10.2514/1.G005610.

[51] Q. Su *et al.*, “Observability Analysis and Navigation Algorithm for Distributed Satellites System Using Relative Range Measurements,” en, *Journal of Systems Science and Complexity*, vol. 31, no. 5, pp. 1206–1226, Oct. 2018, ISSN: 1559-7067. DOI: 10.1007/s11424-018-6096-1.

[52] L. Zhang *et al.*, “Navigation Performance of the Libration Point Satellite Navigation System in Cislunar Space,” en, *The Journal of Navigation*, vol. 68, no. 2, pp. 367–382, Mar. 2015, ISSN: 0373-4633, 1469-7785. DOI: 10.1017/S0373463314000617.

[53] J. Parker *et al.*, “Navigation Between Geosynchronous and Lunar L1 Orbiters,” in *AIAA/AAS Astrodynamics Specialist Conference*, American Institute of Aeronautics and Astronautics. DOI: 10.2514/6.2012-4878.

[54] R. M. McGranaghan *et al.*, “Interplanetary Departure Stage Navigation by Means of Liaison Orbit Determination Architecture,” NTRS Author Affiliations: Colorado Univ., Jet Propulsion Lab., California Inst. of Tech. NTRS Document ID: 20150007228 NTRS Research Center: Jet Propulsion Laboratory (JPL), Kauai, HI, Feb. 2013.

[55] J. S. Parker *et al.*, “Liaison-Supplemented Navigation of a Crewed Vehicle in a Lunar Halo Orbit,” NTRS Author Affiliations: Colorado Univ., Jet Propulsion Lab., California Inst. of Tech. NTRS Report/Patent Number: AAS 13-776 NTRS Document ID: 20150008052 NTRS Research Center: Jet Propulsion Laboratory (JPL), Hilton Head, SC, Aug. 2013.

[56] L. Chen *et al.*, “Orbital Prediction Error Propagation of Space Objects,” en, in L. Chen *et al.*, Eds., Singapore: Springer, 2017, pp. 23–75, ISBN: 9789811029639. DOI: 10.1007/978-981-10-2963-9_2.

[57] Y. Gao *et al.*, “Research on the Effectiveness of Different Estimation Algorithm on the Autonomous Orbit Determination of Lagrangian Navigation Constellation,” en, *International Journal of Aerospace Engineering*, vol. 2016, e8392148, Oct. 2016, ISSN: 1687-5966. DOI: 10.1155/2016/8392148.

[58] J. S. Parker *et al.*, *Low-Energy Lunar Trajectory Design*, en. John Wiley & Sons, Jun. 2014, Google-Books-ID: KlrwAwAAQBAJ, ISBN: 9781118853870.

[59] R. S. Park *et al.*, “Nonlinear Mapping of Gaussian Statistics: Theory and Applications to Spacecraft Trajectory Design,” en, *Journal of Guidance, Control, and Dynamics*, vol. 29, no. 6, pp. 1367–1375, Nov. 2006, ISSN: 0731-5090, 1533-3884. DOI: 10.2514/1.20177.

[60] Y. Tang *et al.*, “Effect of orbital shadow at an Earth-Moon Lagrange point on relay communication mission,” en, *Science China Information Sciences*, vol. 60, no. 11, p. 112 301, Sep. 2017, ISSN: 1869-1919. DOI: 10.1007/s11432-016-9069-9.

[61] E. E. Fowler *et al.*, “Observability Metrics for Space-Based Cislunar Domain Awareness,” en, *The Journal of the Astronautical Sciences*, vol. 70, no. 2, p. 10, Mar. 2023, ISSN: 2195-0571. DOI: 10.1007/s40295-023-00368-w.

[62] T. A. Pavlak *et al.*, “Evolution of the out-of-plane amplitude for quasi-periodic trajectories in the Earth–Moon system,” *Acta Astronautica*, vol. 81, no. 2, pp. 456–465, Dec. 2012, ISSN: 0094-5765. DOI: 10.1016/j.actaastro.2012.07.025.

[63] R. W. Farquhar *et al.*, “Quasi-periodic orbits about the translunar libration point,” en, *Celestial mechanics*, vol. 7, no. 4, pp. 458–473, Jun. 1973, ISSN: 1572-9478. DOI: 10.1007/BF01227511.

[64] D. Folta *et al.*, “Earth–Moon libration point orbit stationkeeping -Theory modeling, and operations,” *Acta Astronautica*, vol. 94, Jan. 2013. DOI: 10.1016/j.actaastro.2013.01.022.

[65] Y. Luo *et al.*, “A review of uncertainty propagation in orbital mechanics,” *Progress in Aerospace Sciences*, vol. 89, pp. 23–39, Feb. 2017, ADS Bibcode: 2017PrAeS..89...23L, ISSN: 0376-0421. DOI: 10.1016/j.paerosci.2016.12.002.

[66] T. A. Pavlak, “Trajectory design and orbit maintenance strategies in multi-body dynamical regimes,” en, Ph.D. dissertation, Purdue University, Jan. 2013.

[67] M. T. Caudill, “A Relative Orbit Determination and Navigation Strategy for Lunar Gateway,” en, M.S. thesis, University of Colorado Boulder, Jul. 2021.

[68] M. Shirobokov *et al.*, “Survey of Station-Keeping Techniques for Libration Point Orbits,” *Journal of Guidance, Control, and Dynamics*, vol. 40, no. 5, pp. 1085–1105, 2017, ISSN: 0731-5090. DOI: 10.2514/1.G001850.

[69] X. Fu *et al.*, “Stochastic optimization for stationkeeping of periodic orbits using a high-order Target Point Approach,” en, *Advances in Space Research*, vol. 70, no. 1, pp. 96–111, Jul. 2022, ISSN: 0273-1177. DOI: 10.1016/j.asr.2022.04.039.

[70] A. Nugmanov *et al.*, “Computer Simulation of Station Keeping Costs of Halo Orbits in Sun-Earth system,” en, *Journal of Physics: Conference Series*, vol. 1740, no. 1, p. 012 020, Jan. 2021, ISSN: 1742-6596. DOI: 10.1088/1742-6596/1740/1/012020.

[71] M. Mahooti, *JPL Development Ephemerides (DE405)_MATLAB code*. Nov. 2020. DOI: 10.13140/RG.2.2.24955.95520.

[72] D. Dirkx *et al.*, “The open-source astrodynamics Tudatpy software - overview for planetary mission design and science analysis,” in *Europlanet Science Congress 2022*, Sep. 2022, EPSC2022–253. DOI: 10.5194/epsc2022-253.

[73] A. Cano *et al.*, “Improving Orbital Uncertainty Realism Through Covariance Determination in GEO,” en, *The Journal of the Astronautical Sciences*, vol. 69, no. 5, pp. 1394–1420, Oct. 2022, ISSN: 2195-0571. DOI: 10.1007/s40295-022-00343-x.

[74] M. E. Lisano, “Comparing Consider-Covariance Analysis with Sigma-Point Consider Filter and Linear-Theory Consider Filter Formulations,” NTRS Author Affiliations: Jet Propulsion Lab., California Inst. of Tech. NTRS Document ID: 20080012709 NTRS Research Center: Goddard Space Flight Center (GSFC), Sep. 2007.

[75] O. Montenbruck *et al.*, *Satellite Orbits: Methods, Models and Applications*. Springer, Jan. 2000, vol. 1, ISBN: 9783540672807. DOI: 10.1007/978-3-642-58351-3.

[76] J. L. Crassidis *et al.*, “Optimal Estimation of Dynamic Systems,” en, in *IEEE Aerospace Conference 2008*, Chapman and Hall/CRC, Apr. 2004, ISBN: 9780203509128. DOI: 10.1201/9780203509128.

[77] S. Akhlaghi *et al.*, “Adaptive adjustment of noise covariance in Kalman filter for dynamic state estimation,” *2017 IEEE Power & Energy Society General Meeting*, pp. 1–5, Jul. 2017. DOI: 10.1109/PESGM.2017.8273755.

[78] T. Lou *et al.*, “Consider unobservable uncertain parameters using radio beacon navigation during Mars entry,” English, *Advances in Space Research*, vol. 55, no. 4, pp. 1038–1050, 2015, ISSN: 0273-1177. DOI: 10.1016/j.asr.2014.11.016.

[79] E. Wan *et al.*, “The unscented Kalman filter for nonlinear estimation,” *Proceedings of the IEEE 2000 Adaptive Systems for Signal Processing, Communications, and Control Symposium (Cat. No.00EX373)*, pp. 153–158, 2000. DOI: 10.1109/ASSPCC.2000.882463.

[80] R. R. Labbe, *Kalman and Bayesian Filters in Python*. GitHub, 2020.

[81] A. D. Dianetti *et al.*, “Application of Observability Analysis to Space Object Tracking,” *AIAA Guidance, Navigation, and Control Conference*, AIAA SciTech Forum, Jan. 2017. DOI: 10.2514/6.2017-1258.

[82] D. Guzzetti *et al.*, “Rapid trajectory design in the Earth–Moon ephemeris system via an interactive catalog of periodic and quasi-periodic orbits,” en, *Acta Astronautica*, Space Flight Safety, vol. 126, pp. 439–455, Sep. 2016, ISSN: 0094-5765. DOI: 10.1016/j.actaastro.2016.06.029.

[83] A. M. Friedman *et al.*, “Determining Debris Characteristics from Observability Analysis of Artificial Near-Earth Objects,” de, 2017.

[84] J. Yim *et al.*, “1 AAS 04-257 autonomous orbit determination for two spacecraft from relative position measurements,” 2004.

[85] Y. Luo *et al.*, “Observability Analysis and Improvement Approach for Cooperative Optical Orbit Determination,” en, *Aerospace*, vol. 9, no. 3, p. 166, Mar. 2022, ISSN: 2226-4310. DOI: 10.3390/aerospace9030166.

[86] X. Zhou *et al.*, “Observability analysis of cooperative orbit determination using inertial inter-spacecraft angle measurements,” *Acta Astronautica*, vol. 210, pp. 289–302, Sep. 2023, ISSN: 0094-5765. DOI: 10.1016/j.actaastro.2023.05.019.

[87] J. Kruger *et al.*, “Observability analysis and optimization for angles-only navigation of distributed space systems,” *Advances in Space Research*, Sep. 2023, ISSN: 0273-1177. DOI: 10.1016/j.asr.2023.08.055.

[88] M. L. Psiaki, “Absolute Orbit and Gravity Determination Using Relative Position Measurements Between Two Satellites,” *Journal of Guidance, Control, and Dynamics*, vol. 34, no. 5, pp. 1285–1297, Sep. 2011, ISSN: 0731-5090. DOI: 10.2514/1.47560.

[89] J. A. Christian, “Relative Navigation Using Only Intersatellite Range Measurements,” en, *Journal of Spacecraft and Rockets*, vol. 54, no. 1, pp. 13–28, Jan. 2017, ISSN: 0022-4650, 1533-6794. DOI: 10.2514/1.A33608.

[90] H.-E. Park *et al.*, “Relative navigation for autonomous formation flying satellites using the state-dependent Riccati equation filter,” en, *Advances in Space Research*, vol. 57, no. 1, pp. 166–182, Jan. 2016, ISSN: 0273-1177. DOI: 10.1016/j.asr.2015.10.009.

[91] I. Chang *et al.*, “High-Fidelity Discrete-Time State-Dependent Riccati Equation Filters for Stochastic Nonlinear Systems with Gaussian/Non-Gaussian Noises,” *2018 Annual American Control Conference (ACC)*, pp. 1132–1137, Jun. 2018. DOI: 10.23919/ACC.2018.8431771.

[92] F. O. Hoffman *et al.*, “Propagation of Uncertainty in Risk Assessments: The Need to Distinguish Between Uncertainty Due to Lack of Knowledge and Uncertainty Due to Variability,” en, *Risk Analysis*, vol. 14, no. 5, pp. 707–712, 1994, ISSN: 1539-6924. DOI: 10.1111/j.1539-6924.1994.tb00281.x.

[93] S. K. Flegel *et al.*, “State Uncertainty Normality Detection,” en, *The Journal of the Astronautical Sciences*, vol. 67, no. 3, pp. 1044–1062, Sep. 2020, ISSN: 2195-0571. DOI: 10.1007/s40295-019-00201-3.

[94] D. K. Geller, “Linear Covariance Techniques for Orbital Rendezvous Analysis and Autonomous Onboard Mission Planning,” *Journal of Guidance, Control, and Dynamics*, vol. 29, no. 6, pp. 1404–1414, Nov. 2006, ISSN: 0731-5090. DOI: 10.2514/1.19447.

[95] D. K. Geller *et al.*, “Event Triggers in Linear Covariance Analysis with Applications to Orbital Rendezvous,” *Journal of Guidance, Control, and Dynamics*, vol. 32, no. 1, pp. 102–111, Jan. 2009, ISSN: 0731-5090. DOI: 10.2514/1.36834.

[96] C. McLeod, “Effect of nonlinearities on orbit covariance propagation,” M.S. thesis, Naval Postgraduate School, Sep. 2013.

[97] R. S. Park *et al.*, “Nonlinear Semi-Analytic Methods for Trajectory Estimation,” *Journal of Guidance, Control, and Dynamics*, vol. 30, no. 6, pp. 1668–1676, Nov. 2007, ISSN: 0731-5090. DOI: 10.2514/1.29106.

[98] Z. Yang *et al.*, “Nonlinear Analytical Uncertainty Propagation for Relative Motion near J2-Perturbed Elliptic Orbits,” en, *Journal of Guidance, Control, and Dynamics*, vol. 41, no. 4, pp. 888–903, Apr. 2018, ISSN: 0731-5090, 1533-3884. DOI: 10.2514/1.G003071.

[99] Z. Yang *et al.*, “Nonlinear semi-analytical uncertainty propagation of trajectory under impulsive maneuvers,” en, *Astrodynamics*, vol. 3, no. 1, pp. 61–77, Mar. 2019, ISSN: 2522-0098. DOI: 10.1007/s42064-018-0036-7.

[100] S. Boone *et al.*, “Orbital Guidance Using Higher-Order State Transition Tensors,” *Journal of Guidance, Control, and Dynamics*, vol. 44, no. 3, pp. 493–504, Mar. 2021, ISSN: 0731-5090. DOI: 10.2514/1.G005493.

[101] S. Boone *et al.*, “Directional State Transition Tensors for Capturing Dominant Nonlinear Effects in Orbital Dynamics,” *Journal of Guidance, Control, and Dynamics*, vol. 46, no. 3, pp. 431–442, 2023, ISSN: 0731-5090. DOI: 10.2514/1.G006910.

[102] A. Haapala, “Trajectory design using periapse maps and invariant manifolds,” M.S. thesis, Purdue University, Jan. 2010.

[103] S. Speretta *et al.*, “Designing the Radio Link for a Lunar CubeSat: The LUMIO Case,” en, *72nd International Astronautical Conference*, 2021.